BIRL
Northwestern University
1801 Maple Avenue
Evanston, IL 60201-3135

July 7, 1995

FINAL REPORT

NASA - LEWIS RESEARCH CENTER

ENTITLED

CVD FIBER COATINGS FOR Al_2O_3/NiAl COMPOSITES

by

Daniel E. Boss
Research Scientist

TABLE OF CONTENTS

ACKNOWLEDGEMENT 1

1.0 SUMMARY 2

2.0 INTRODUCTION 3

2.1 Limitations of Continuous Fiber Composites 4
2.2 Fiber Coatings for Al_2O_3/NiAl Composites 5
2.3 Fiber Coating by Chemical Vapor Deposition 7

2.3.1 CVD Molybdenum 7
2.3.2 Functionally Gradient Material 8

3.0 RESULTS AND DISCUSSION 10

3.1 Molybdenum Fiber Coatings 10

3.1.1 Experimental System 10
3.1.2 Deposition Trials 12

3.2 CVD Functionally Gradient Material 34

3.2.1 Reactor Design and Installation 34
3.2.2 CVD Alumina 35
3.2.3 CVD NiAl and FGM 38

3.3 Nickel/Yttria Coatings 47

3.3.1 Experimental System 47
3.3.2 Nickel/Yttria Coating Development 49

4.0 CONCLUSIONS AND RECOMMENDATIONS 52

4.1 Conclusions 52
4.2 Recommendations 52

5.0 FUTURE WORK 54

6.0 REFERENCES 55

LIST OF FIGURES

Figure 1. Predicted Residual Stresses in Al_2O_3/NiAl.. 6

Figure 2. Schematic of CVD Molybdenum Reactor 11

Figure 3. 10 μm Coating from Sample 195-21-1B 13

Figure 4. Sample 195-21-2 Produced at Higher Partial Pressure 14

Figure 5. Sample 195-21-5B Produced at 873K 14

Figure 6. Sample 195-25-1 Produced at 773K 15

Figure 7. Sample 195-25-4 Processed with Argon Diluent 16

Figure 8. Auger Analysis of Sample 195-25-4 16

Figure 9. XRD Analysis of Sample 195-29-2 showing Mo_2C 18

Figure 10. XRD Analysis of Sample 195-33-1 Produced at 673K 19

Figure 11. XRD of As-Deposited Sample 195-36-2 20

Figure 12. Morphology of Sample 195-36-2 After Heat Treatment 21

Figure 13. XRD Analysis of Sample 195-36-2 After Heat Treatment 22

Figure 14. Sample 195-62-3 with 4-μm Mo-O-C from Start of Run 23

Figure 15. Sample 195-92-4 with 4-μm Mo-O-C from end of Run 23

Figure 16. Morphology of Sample 195-74 24

Figure 17. Columnar Structure of Sample 195-74 24

Figure 18. Start of Second Layer for 5-μm Mo Coating 26

Figure 19. End of Second Layer for 5-μm Mo Coating 26

Figure 20. Heat-Treated Mo Coating With Dendritic Structure 27

Figure 21. 5-μm Mo Coating Debonded from Fiber 27

Figure 22. Columnar Growth and Porosity in 5-μm Mo Coating 28

Figure 23. Smooth Morphology of Sample 259-7 28
Figure 24. Dense and Columnar Structure of Sample 259-7 29
Figure 25. 20 μm Coating from Sample 257-9 29
Figure 26. Growth Structure of 20-μm Mo-O-C Coating 30
Figure 27. 12 μm Coating from Sample 257-20 31
Figure 28. Porous and Adherent Mo on Sapphire 31
Figure 29. Porosity in 10-μm Mo Sample 32
Figure 30. Mo-O-C for Second Lot of 5 μm Coating 33
Figure 31. Heat Treated Coating 33
Figure 32. FGM Reactor Schematic 34
Figure 33. Al_2O_3 with Island Growth Morphology. 36
Figure 34. Al_2O_3-Coated Al_2O_3 Fiber. 37
Figure 35. Al_2O_3 Coating from Sample 195-18 37
Figure 36. Sample 195-68-1 Produced at 523K 39
Figure 37. Sample 195-68-2 with 76 a/o Al and 24 a/o Ni 39
Figure 38. Sample 195-68-3 Produced at 623K. 41
Figure 39. Sample 195-68-4 with 83 a/o Al and 17 a/o Ni 41
Figure 40. Sample 195-68-5 Produced at 723K 42
Figure 41. Sample 195-72-4 with 52 a/o Al and 48 a/o Ni 42
Figure 42. 2 μm to 3 μm Coating on Sample 195-76 44
Figure 43. XRD Pattern from Sample 195-76 45
Figure 44. Sample 195-81 with 11 a/o Nickel 46

Figure 44. Sample 195-81 with 11 a/o Nickel 46

Figure 45. Coating Produced in FGM Sample 195-87 47

Figure 46. CVD Nickel System Schematic 48

Figure 47. CVD Nickel Coating Produced in 40 Minutes 50

Figure 48. Nickel Coating Produced at 393K 51

Figure 49. Nickel/Y_2O_3 Coating 51

LIST OF TABLES

Table 1. Phases Present in Sample 195-76 44

ACKNOWLEDGEMENT

Many people contributed to this program, and I would like to thank the following BIRL staff, Mark Madsen, Michael Wieczorek, David Pedrazzani, and Brent Forbes, for their help throughout the project. A special thanks goes to Dr. Randy Bowman, our technical monitor at NASA - LeRC, for his support, advice, and patience throughout our effort.

1.0 SUMMARY

While sapphire-fiber-reinforced nickel aluminide (Al_2O_3/NiAl) composites are an attractive candidate for high-temperature structures, the significant difference in the coefficient of thermal expansion between the NiAl matrix and the sapphire fiber creates substantial residual stresses in the composite. This study seeks to produce two fiber-coating systems with the potential to reduce the residual stresses in the sapphire/NiAl composite system. The fiber coatings selected for this program were molybdenum and an Al_2O_3-NiAl functionally gradient material (FGM). Molybdenum was selected as a candidate compliant layer, which would plastically deform to reduce the strain between the fiber and matrix. The FGM interface was selected as a compensating layer in which the gradual change in composition between the fiber and matrix would distribute the thermal strain across a larger area.

Chemical vapor deposition (CVD) was used to produce both the compensating and compliant fiber coatings for use in sapphire/NiAl composites. A special reactor was designed and built to produce the FGM and to handle the toxic nickel precursors. While some success was achieved in the deposition of NiAl by metalorganic CVD techniques, the process was not repeatable, and the FGM effort was dropped. In place of the FGM, CVD nickel coatings, approximately 3-μm, 5-μm, and 10-μm thick, were produced in a batch reactor. The nickel-coated fiber was then over-coated with yttria (Y_2O_3), using a solution process, to prevent reaction between the NiAl matrix and the nickel during consolidation.

The molybdenum coatings were deposited using a two-step process. A Mo-O-C layer was first deposited from molybdenum hexacarbonyl, and then in a separate operation, this was reduced in hydrogen to form molybdenum. This process was successfully used to produce 500-foot lengths of fiber with coating thicknesses of approximately 3 μm, 5 μm, and 10 μm. Both the nickel- and molybdenum-coated fibers were delivered to NASA for testing and evaluation.

2.0 INTRODUCTION

The B2 intermetallic compound, nickel aluminide (NiAl), is being considered for a variety of high-temperature applications, ranging from chemical-processing equipment to gas-turbine engine components. The diversity of the potential applications for NiAl stems from its uncommon blend of high-melting temperature, high-specific mechanical properties, oxidation resistance, and high-temperature toughness. As is the case with many intermetallic compounds, NiAl is brittle at room temperature but exhibits a brittle-to-ductile-transition temperature (BDTT) of approximately 550K. This high-temperation transition from brittle to ductile behavior presents a barrier to the use of NiAl components because of a limited damage tolerance at ambient temperature.

To address the concerns with its high-temperature strength and low-temperature toughness, the addition of continuous-fiber reinforcements to NiAl have been investigated. Several investigators (1-7) have evaluated the mechanical properties of NiAl-matrix composites reinforced with tungsten (W), molybdenum (Mo), or sapphire (Al_2O_3) fibers, and they found a strong correspondence in the strength of the composite to the strength of the fiber-matrix bond. The greatest strengthening of NiAl-matrix composites was achieved using either Mo or W fibers (1,2,5-7), with the Mo retaining ductility and providing some additional toughness to the composite (2,7). While the W and Mo fibers do strengthen the NiAl matrix, their high densities and poor oxidation resistance make their use in a commercial composite system highly unlikely.

The studies evaluating Al_2O_3 fibers concluded that the weak bond strength between the Al_2O_3 fiber and NiAl matrix may provide toughening at room temperature, but the fibers did not contribute as much as predicted to the strength of the composite (4-7). While the Al_2O_3-reinforced NiAl has a higher specific tensile strength than the W-reinforced system (6), it has been found (3) that the Al_2O_3 fiber may completely debond from the NiAl matrix at temperatures of approximately 900K. This suggests that only the clamping forces, caused by the coefficient of thermal expansion (CTE) mismatch between the fiber and matrix, provide load transfer to the fiber at lower temperatures.

Recently Bowman (2) has found that a dramatic increase in bond strength between the Al_2O_3 fiber and the NiAl matrix can be achieved by eliminating the organic binders from the matrix-powder cloth. The strength of the Al_2O_3/NiAl interface was evaluated using a fiber push-out test which can apply loads of up to 280 MPa to the fiber. Using the fiber push-out process, the Al_2O_3/NiAl composites fabricated by Bowman, using the standard powder cloth method, had a room temperature interfacial strength ranging from 30 MPa to 100 MPa, while the composites fabricated without a binder had strengths of over 280 MPa. Just as importantly, the interfacial strength of the binder-free composite was retained after 1000 thermal cycles between 400K and 1300K. While this simple modification of the powder metallurgy process for Al_2O_3/NiAl composites addresses the poor fiber-matrix bond strength of these composites, other limitations remain.

2.1 Limitations of Continuous Fiber Composites

Two major hurdles for the continued development of Al_2O_3/NiAl composites are their poor toughness below the BDTT of the matrix and the residual stresses due to the large thermal-expansion mismatch between the Al_2O_3 fiber and NiAl matrix. Bowman (2) found that even the weakly bonded Al_2O_3/NiAl composites, in which toughening by fiber pull-out may be expected, failed in a brittle manner. He proposed that critical defects were introduced into the brittle NiAl matrix when the Al_2O_3 fibers failed. This low toughness must be addressed before Al_2O_3/NiAl composites can be applied in aerospace structures.

The other unresolved issues are the large residual stresses (radial, axial, and circumferential) present in the Al_2O_3/NiAl system. These stresses are produced on cooling the composite from the consolidation temperature of approximately 1473K. The CTE of NiAl is approximately 16 x 10^{-6}/K, while that of Al_2O_3 is between 8 x 10^{-6}/K and 9 x 10^{-6}/K in the axial and radial directions, respectively. The residual stresses in the Al_2O_3/NiAl system have been the focus of several studies (8-11). Wright (8) measured the residual thermal strains in the Al_2O_3/NiAl system using neutron diffraction, and he found matrix strains of 0.0014 in the longitudinal and 0.0004 in the transverse directions. Using a NiAl modulus of 200 GPa, these strains correlate to stresses of 350 MPa longitudinal and -100 MPa transverse. This longitudinal stress is greater than the reported room-

temperature yield stress for NiAl (approximately 120 MPa) (12). In tensile testing of Al_2O_3/NiAl composites, Bowman (2) found a change in modulus of the composites at approximately 60 MPa, which translates to a matrix stress of only 41 MPa. After metallographic examination of the samples, he proposed that the reduced yield point of the matrix was the result of residual stresses in the matrix.

2.2 Fiber Coatings for (Al_2O_3)/NiAl Composites

A recent topic of high interest has been the use of fiber coatings to modify the residual stress of a composite. Numerous studies (10,11,13-18) have been performed to develop models to predict both the residual stress state in composites and the effect of fiber coatings on the residual stress using a variety of micromechanical methods. The models used in these studies are usually based on concentric cylinders. Others (8-11,19,20) have measured the residual stresses in intermetallic composites. Two basic premises (13-18) for reducing the residual stress have emerged from these efforts. The consensus is that the use of a compliant- and/or compensating-fiber coating should reduce the CTE-generated, residual stresses in composites. A compliant-fiber coating accommodates the CTE-mismatch strain through plastic deformation, so a compliant layer should have a low-yield stress and exhibit low-work hardening. A compensating layer is, generally, a material with a higher CTE than either the matrix or fiber. Thus, on cooling from the consolidation temperature, the fiber coating would shrink more than the matrix and the fiber and reduce the residual stress. In both cases the fiber coating thickness must be optimized for the particular composite system.

As an example of the expected change in residual stress state through the use of fiber coatings, the work of Arnold (15) and Misra (3) will be briefly discussed. Both studies examined the axial, radial, and circumferential stresses in different composite systems. Arnold examined a Ti_3Al + Nb alloy reinforced with SiC fibers. To reduce the residual stresses of this composite system, fiber coatings of Cu (compensating), Nb (compliant), and Cu/Nb were modeled. These coatings significantly reduced the tensile stresses adjacent to the fiber, with the compensating coating having the greatest effect. This residual stress reduction would be expected to improve the thermomechanical fatigue behavior of the composite system.

Misra (3) evaluated the effect of fiber coatings for the Al_2O_3/NiAl system and summarized his results for the axial, radial, and circumferential stresses in a chart (Figure 1). The high-thermal expansion of NiAl and its reactivity (21) limit the choice of materials for compensating and compliant layers. The candidate coating materials listed in Figure 1 provide only a small reduction in residual stress of the composite. Misra also proposes the use of an 8- μm to 10-μm coating of Mo to enhance the room temperature toughness of the Al_2O_3/NiAl

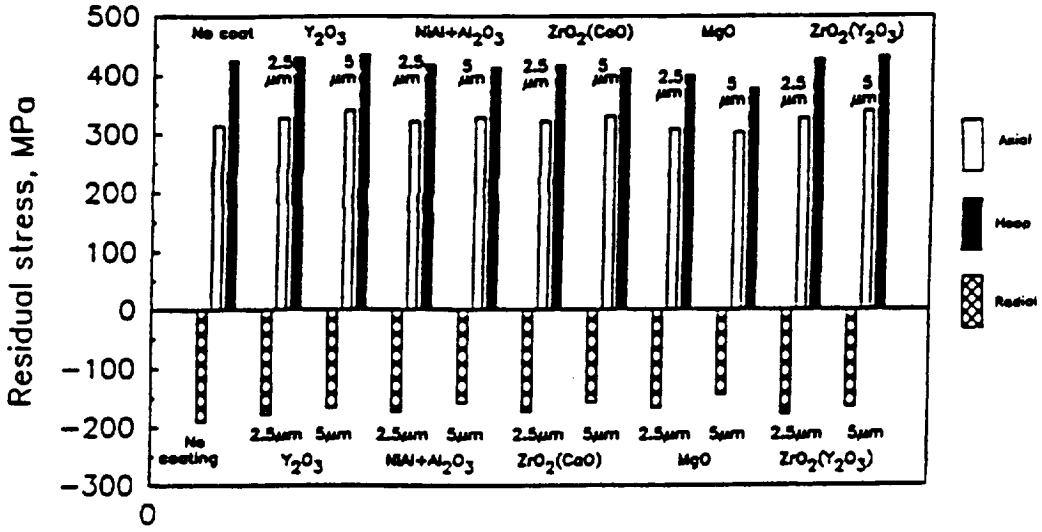

Figure 1. Predicted Residual Stresses in Sapphire/NiAl

system. His work also showed an increase in the debond stress and frictional-shear stress for Mo-coated sapphire versus uncoated fiber in NiAl composites. The debond stress and frictional-shear stress measured by Misra (3) were 110 MPa and 65 MPa, respectively, for the Mo-coated fiber, while the uncoated fiber had values of 58 MPa and 48 MPa, respectively.

After reviewing the available information, molybdenum and an Al_2O_3-NiAl functionally-gradient material (FGM) were selected for development and production in this program because of their potential to reduce the residual stresses in the sapphire/NiAl composite systems. Molybdenum is an example of a compliant layer, which may deform to reduce the strain between the fiber and matrix. The FGM may act as a compensating layer in which the gradual change in composition

between the fiber and matrix distributes the thermal strain across a larger volume. Both of these coating systems were deposited by chemical vapor deposition.

2.3 Fiber Coating by Chemical Vapor Deposition

A key aspect in the development of any interfacial coating is that the fiber must retain its strength after the coating has been applied. Many chemical vapor deposition (CVD) reactions utilize precursors that contain halides and produce by-products such as HCl and HF. The HCl and HF by-products have been shown to etch the sapphire-fiber surface and significantly degrade its strength. Thus, the use of metallorganic precursors was specifically proposed for this effort. The other goal set forth for this effort was to evaluate three thicknesses of both the compliant- and compensating-interfacial coatings. Molybdenum was selected as the compliant-layer material since NASA had promising recent results with this material (2,3,7). We had proposed several candidate compensating coating systems for possible use in this project, and NASA selected the FGM option for this effort, even though they previously had disappointing results when sputtering was used to make a pseudo-FGM coatings (22). Both interface systems were to be deposited as 3-μm, 5-μm, and 10-μm coatings on sapphire fiber. All CVD coatings were to be deposited in hot-wall reactors specifically designed for coating continuous fibers. Deposition of the molybdenum coatings was performed in one of BIRL's standard fiber-coating reactors, while the FGM experiments were performed using a system specifically designed for this project. The FGM system was installed in a walk-in hood because of the safety requirements for working with volatile nickel compounds.

2.3.1 CVD Molybdenum

Molybdenum is commonly deposited by CVD from either its pentachloride or hexaflouride-compound, but these materials would not be suitable for this effort because of the potential of fiber degradation by the halide by-products. While not as widely used as the halide processes, molybdenum is also deposited by CVD using the carbonyl reaction (23-33). A comprehensive study of this process was performed by Lander and Germer (29). The molybdenum hexacarbonyl (MHC) reaction, shown in Equation 1, appears straight forward:

1) $$Mo(CO)_{6(g)} \rightarrow Mo_{(s)} + 6CO_{(g)}$$

but several side reactions occur which limit the deposition envelope that produces pure metal. The primary side reaction is the disproportionation of CO to carbon and CO_2 (29,30). Without careful control of the carbonyl partial pressure, molybdenum carbide and/or molybdenum oxide may be deposited instead of the metal (27,29,30). The formation of oxycarbides has also been reported (31).

To control the incorporation of carbon and oxygen, additions of water vapor, hydrogen, CO_2, and H_2S have all been used with varying degrees of success (29). The deposition reaction occurs in the temperature range of 473K to 1073K, with carbon and oxygen incorporation at lower temperatures above 773K (29). Initial thermodynamic modeling, using the on-line Facility for the Analysis of Chemical Thermodynamics (F*A*C*T) (34), of the MHC process was performed for this project. The modeling confirmed the results of the cited studies, and indicated that CO partial pressures of less than 150 Pa are necessary to produce Mo directly from MHC. The conditions identified from this modeling effort were used as the starting point for the development of processing conditions for Mo coatings on the sapphire fibers. Once optimized deposition conditions were identified, sapphire fiber samples were then to be coated with 3 μm, 5 μm, and 10 μm of Mo.

2.3.2 Functionally Gradient Material

Typically, a compensating layer will have a coefficient of thermal expansion higher than either the matrix or the fiber and, thus, reduce the residual stresses in the composite. After discussions with NASA personnel, it was decided that a FGM consisting of Al_2O_3-NiAl may act as a compensating layer for the Al_2O_3/NiAl composites. It was thought that forming the Al_2O_3-NiAl FGM, with the Al_2O_3 adjacent to the fiber, would eliminate the abrupt CTE change between the fiber and the matrix and, therefore, reduce the residual-stress gradient in the composite. Only a few studies (35-37) have been reported on FGM coatings produced by CVD, and they dealt solely with the C-SiC system which has only a single deposition variable.

After examining potential deposition routes to the Al_2O_3-NiAl FGM, two potentially independent deposition reactions, shown in Equations 2 and 3, were utilized:

$$2)\quad 2Al(OC_3H_7)_{3(g)} \rightarrow Al_2O_{3(s)} + 3C_3H_7OH_{(g)} + 3C_3H_{6(g)}$$

$$3)\quad Ni(C_5H_5)_{2(g)} + Al(C_4H_9)_{3(g)} \rightarrow NiAl_{(s)} + C_xH_{y(g)}$$

Excess hydrogen was added in both reactions to suppress the decomposition of the hydrocarbon by-products. While the aluminum isopropoxide reaction (Equation 2) is used widely (38-44) to deposit alumina at temperatures from 523K to 1173K, a polycrystalline-alumina coating adjacent to the fiber was expected to degrade the fiber strength. The first task in this portion of the project was to produce 100 feet of alumina-coated sapphire for NASA evaluation.

No studies were found where NiAl had been formed by CVD using only gaseous precursors. Instead, all references found on the deposition of NiAl coatings by CVD referred to the formation of aluminide conversion coatings on nickel or superalloy substrates (45,46) using aluminum chlorides. In this project, nickelocene ($Ni(C_5H_5)_2$) was selected as the nickel precursor. Several studies (47-49) have used nickelocene to produce nickel films at temperatures from 573K to 773K. Nickel carbonyl was considered for this effort, but it is highly toxic and its greater volatility presented serious safety concerns. It was projected that deposition of Ni with Al, from tri-isobutyl aluminum, (Equation 3) at temperatures of 673K to 773K will either form NiAl directly, or by depositing Ni and Al in the correct ratio they will react to form NiAl if heated above approximately 933K. Thermodynamic modeling using the F*A*C*T system verified that the direct deposition of NiAl at temperatures above 500K was thermodynamically possible.

As with the molybdenum reaction, all precursors for the FGM were metallorganics and contained no halides. The largest assumption in this project was that these reactions would proceed along independent mechanisms. If the reactions did interact, a range of other reaction products, including NiO, and $NiAl_2O_4$, were possible. To minimize the risk involved in the development of the FGM, it was decided to perform three sequential efforts: 1) demonstrate polycrystalline

alumina on sapphire, 2) demonstrate CVD NiAl, and 3) develop Al_2O_3-NiAl FGM. After developing CVD parameters, samples of sapphire fiber were to be coated with 3-μm, 5-μm, and 10-μm layers of the FGM.

3.0 RESULTS AND DISCUSSION

3.1 Molybdenum Fiber Coatings

3.1.1 Experimental System

The continuous fiber-coating system used for the molybdenum coating task is shown schematically in Figure 2. This system is used to coat both monofilament and multifilament fibers, and it can process up to three fibers simultaneously. The three-zone furnace is capable of 1473K, and each zone has its own temperature controller. Gas flows and pressures were controlled using standard MKS process control equipment, such as mass flow meters and capacitance manometers. The water-vapor transport was controlled using a bubbler equipped with a pressure-control loop, which kept the pressure within the bubbler constant throughout the process. The MHC was loaded into a fluidized-bed sublimator. The temperature of the sublimator and the flow of carrier-gas flow rate were used to control the transport of the MHC. Argon was used as the carrier gas for both the MHC and water. An argon purge into each end chamber kept these enclosures at a pressure higher than the deposition section, which prevented contamination of the fiber and fiber-handling equipment by the MHC and its by-products. The pumping system consisted of an Edwards M40 equipped with a roots-type blower, which was backed by a venturi to draw the gases into a scrubbing system. The reactor-exhaust line contained several traps to collect condensable materials before they reached the pumping system. The fiber-winding system provided for independent speed and winding-pitch control for each channel.

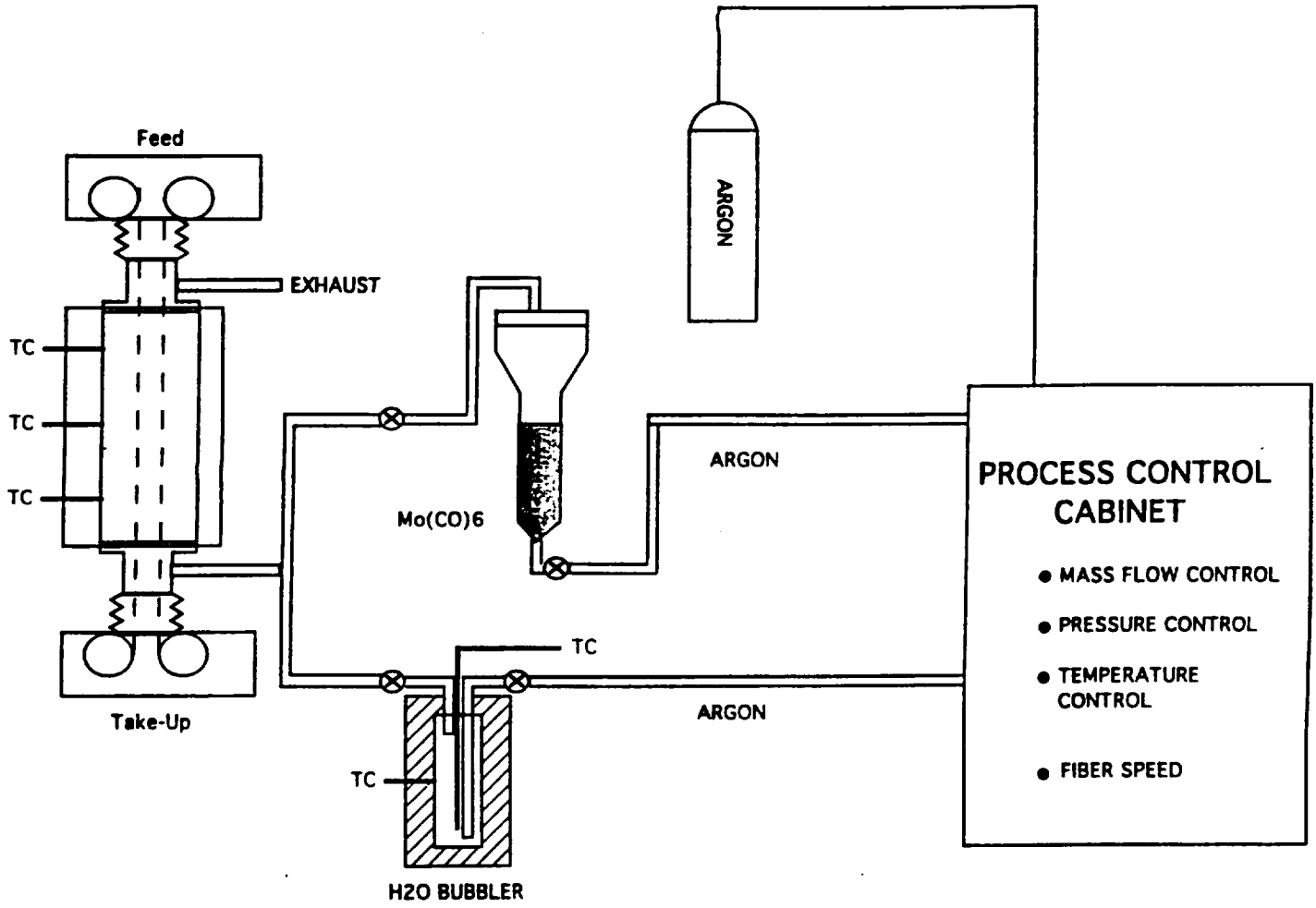

Figure 2. Schematic of CVD Molybdenum Reactor

3.1.2 Deposition Trials

Initial tests focused on determining the temperature and carrier-gas flow effects on the MHC transport rate from the fluid-bed sublimator. Under conditions of ambient temperature (293K), 670 Pa (5 torr) sublimator pressure, and 0.5 standard-liters-per-minute (SLPM) flow of argon carrier gas, approximately 8.5 grams of MHC were transported in 75 minutes. At 323K, 0.5 SLPM argon, and 4.4 KPa (33 torr) sublimator pressure, approximately 3.9 grams of MHC were transported in 30 minutes. Using the vapor pressure curve from Lander and Germer (29), these values correspond to a fluid-bed sublimator efficiency of approximately 63 percent. This efficiency was used to calculate MHC partial pressures and precursor ratios for all remaining processing runs.

Initial deposition runs focused on trying to form Mo directly from the MHC. From the literature review and our own thermodynamic calculations, it was determined that a partial pressure of carbon monoxide (pCO) of less than 150 Pa was required to deposit Mo. A series of static runs were performed at temperatures of 773K (500°C) and 873K (600°C) and pCO values ranging from 0.33 Pa to 550 Pa (2.5×10^{-2} torr to 4.1 torr) to screen the behavior of the MHC. Sections of the fibers coated in these runs are shown in Figures 3 - 5. Sample 195-21-1B was produced in a 30-minute run at a pCO of 0.33 Pa resulting in a coating (Figure 3) approximately 10-μm thick with a moderately smooth morphology. The coating apparently had significant residual stresses, since it cracked axially along the fiber. The MHC flow and pCO (to 2 Pa) were increased for Run 195-21-2 and the growth rate increased significantly, with a 40 μm coating (Figure 4) produced in the 15-minute run. Sample 195-21-5B, at a processing temperature of 873K and a pCo of 550 Pa, yielded a rough and columnar coating over 100-μm thick (Figure 5) in 15 minutes. Preliminary screening of these coatings, using Vickers hardness testing, revealed hardness numbers ranging from 300 to over 850. These values indicated that the coatings contained significant amounts of either molybdenum oxides or molybdenum carbides, since pure Mo has a Vickers hardness value of approximately 200. The oxide or carbide phases were likely produced by the disproportionation of CO as described previously.

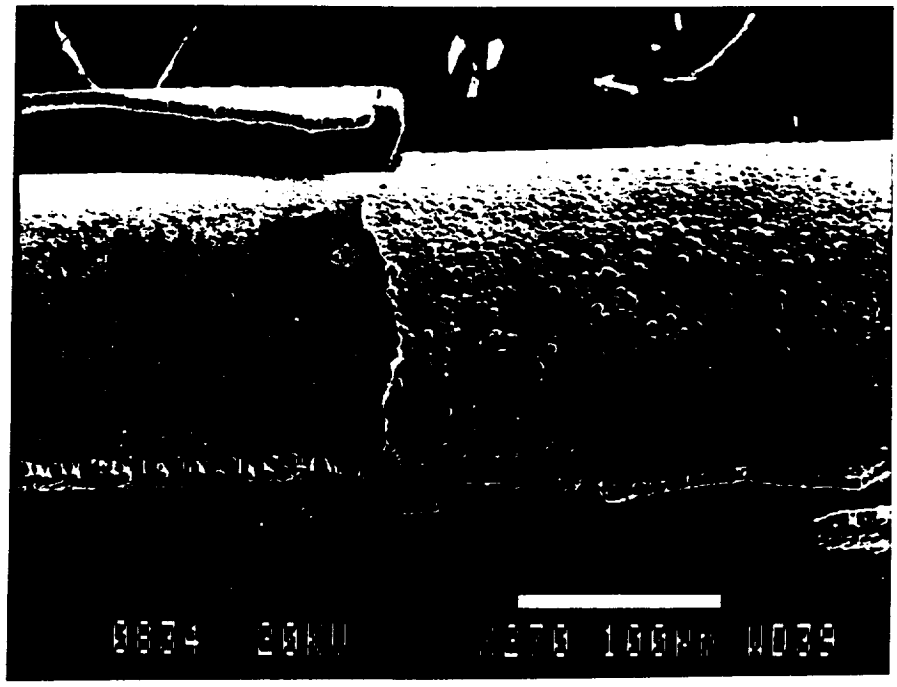

Figure 3. 10 μm Coating from Sample 195-21-1B

The coating rates achieved at the lower pCO levels, which were necessary to produce purer Mo coatings, were not suitable for the production of the hundreds of feet of continuous fiber desired for this program. This realization, and the results of Lander and Germer, led to the addition of water vapor to the reactant stream. If the amount of water vapor added to the gas stream could be balanced with the disproportionation reaction of CO, the water would prevent the formation of carbides in the coating. Calculations using F*A*C*T showed that, theoretically, the water vapor level could be adjusted to produce Mo. However, in our experiments, there was enough variability to the flow of the MHC that we could not obtain a purely metallic deposit. Sample 195-25-1 (Figure 6) was produced at 773 using carrier gas flows of 0.5 SLPM and 0.1 SLPM of Ar through the fluid-bed MHC sublimator and the water bubbler, respectively.

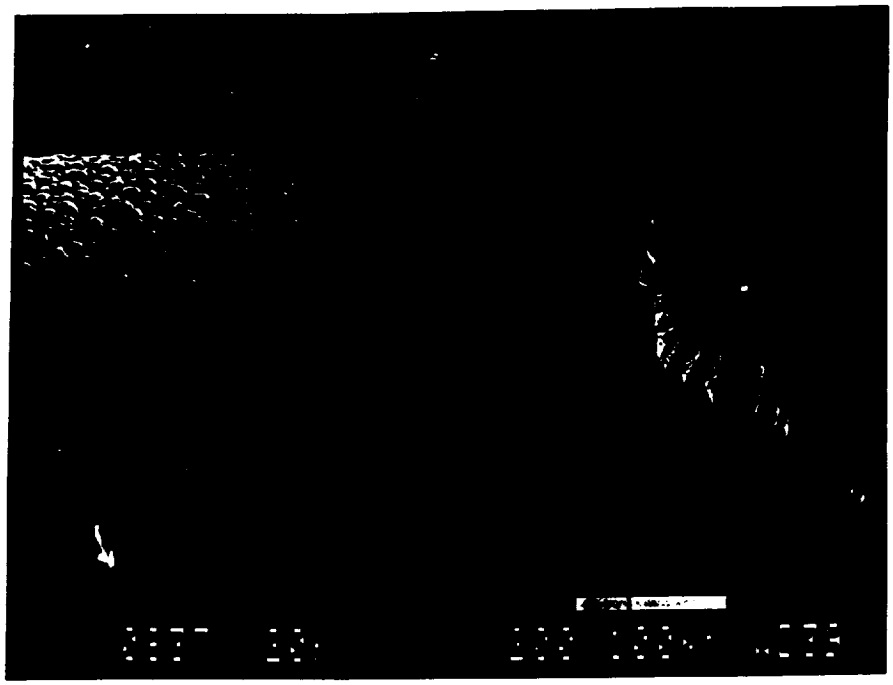

Figure 4. Sample 195-21-2 Produced at Higher Partial Pressure

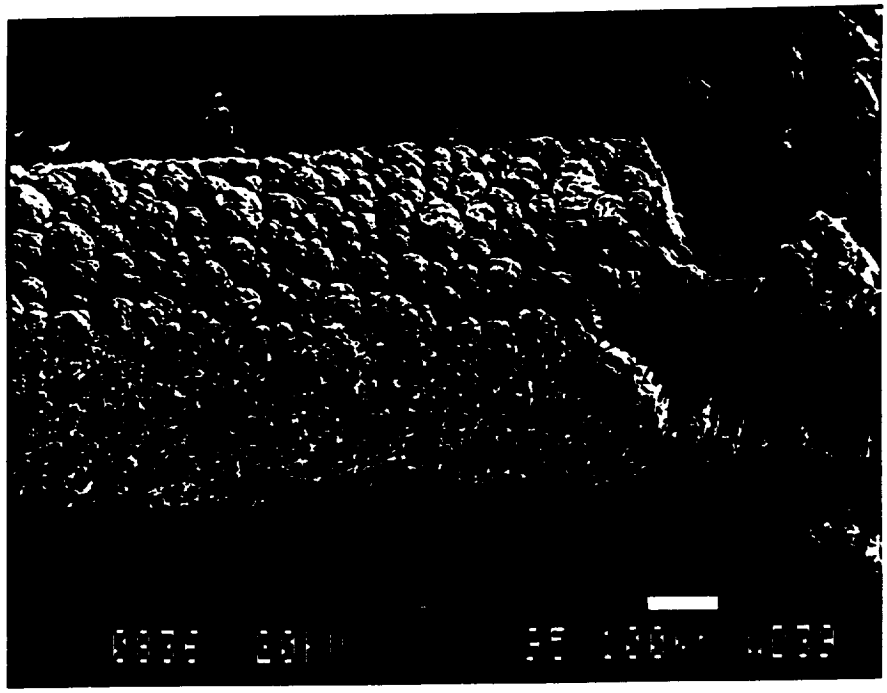

Figure 5. Sample 195-21-5B Produced at 873K

Energy dispersive spectroscopy (EDS) of this 67-μm thick coating revealed only Mo, but this analysis technique can not detect elements below sodium (Z=11). When this sample was heat treated in vacuum at 1273K, the coating sublimed from the fiber, which indicated that the coating contained significant amounts of oxygen. Run 195-25-4 was made at 873K, with an additional 2.1 SLPM Ar as a dilutant, and produced a coating of only 7 μm (Figure 7). This coating was analyzed using Auger electron spectroscopy (AES) (Figure 8), which revealed Mo, oxygen, and minor amounts of carbon and nitrogen.

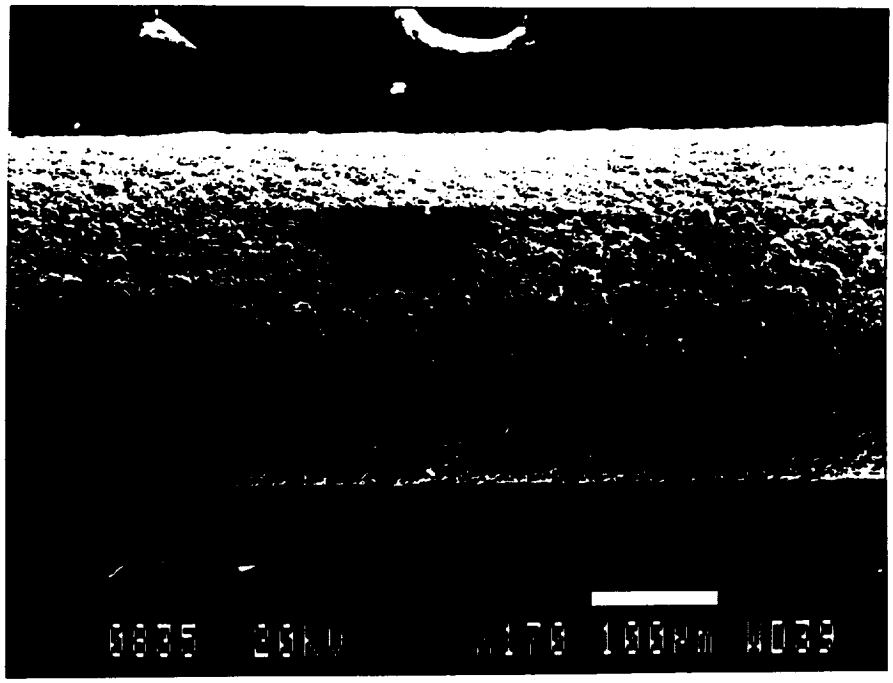

Figure 6. Sample 195-25-1 Produced at 773K

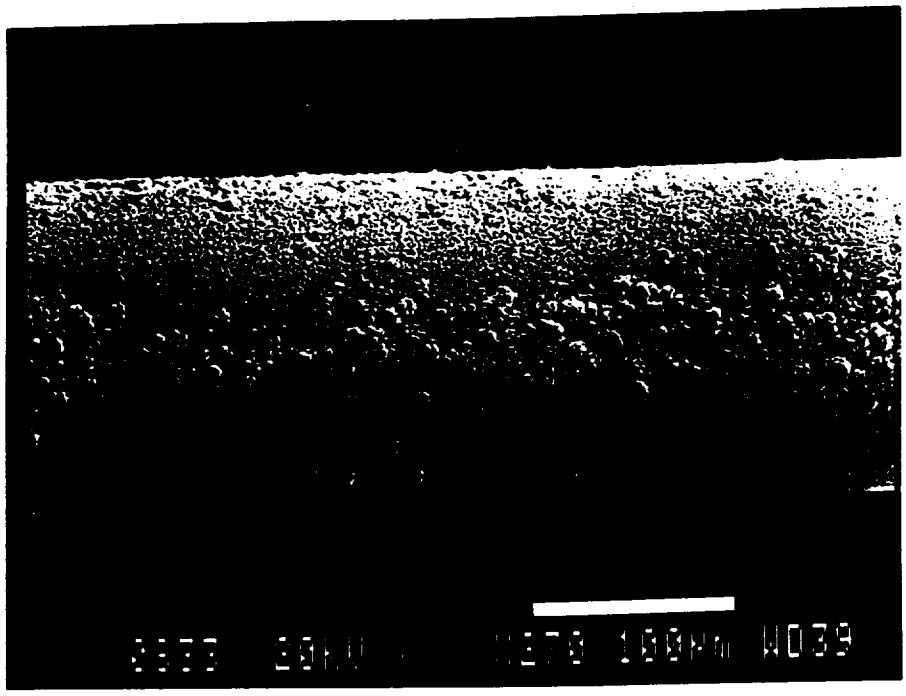

Figure 7. Sample 195-25-4 Processed with Argon Diluent

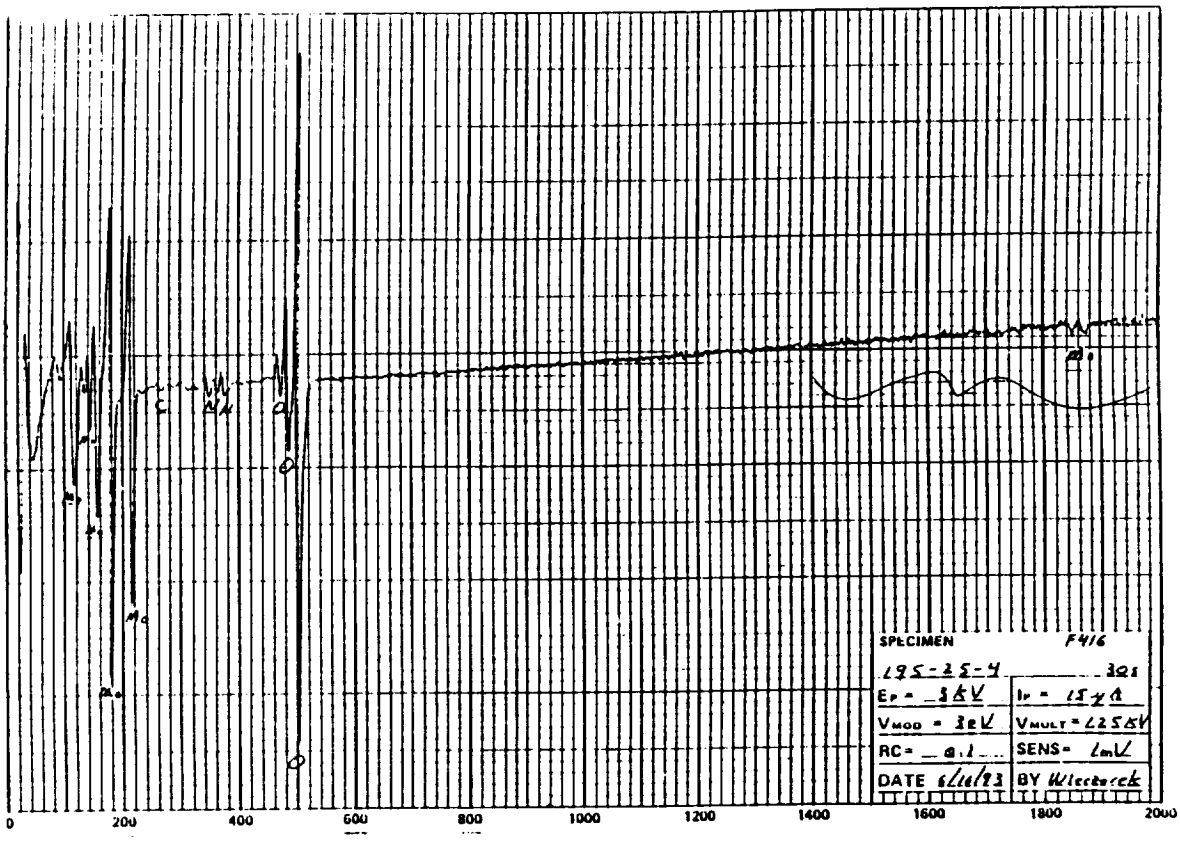

Figure 8. Auger Analysis of Sample 195-25-4

Several more attempts were made to produce a Mo coating using just the MHC. A typical example was Sample 195-29-2. This coating was produced at 773K, using 0.5 SLPM of Ar through the sublimator and a pCO of 35 Pa (0.26 torr). X-ray diffraction (XRD) analysis of this coating (Figure 9) revealed predominantly Mo_2C, and, possibly, a minor amount of Mo. When similar runs were made at 673K, only amorphous coatings were produced. Sample 195-33-1 was typical of this result, as can be seen by the XRD spectra for this sample (Figure 10). The peak counts for this sample were very low and had no recognizable pattern, but some of the peaks can be approximated to the compounds Mo-O-C, Mo-O, and Mo-C. However, the coating thickness was sufficient to shield the sapphire fiber from the x-ray beam, which typically yields a strong response of 50,000 to 60,000 counts-per-minute at 2θ values of approximately 40.5° and 68.3°. The formation of Mo-O-C coatings was also reported by Kmetz (31) in his efforts to produce Mo coatings from MHC. Kmetz reported that the Mo-O-C material could be reduced by hydrogen to form pure Mo coatings. As a test of this method, Sample 195-36-2 was produced at 773K. The sample had a nearly amorphous XRD spectra (Figure 11) with only one or two "peaks". This sample was heat treated in one atmosphere of hydrogen for 30 minutes and re-examined. The microstructure had changed from a moderately smooth to a faceted coating (Figure 12), while the XRD spectra (Figure 13) showed distinct peaks at 2θ values corresponding to Mo.

Once this two-step process had been demonstrated, 152 meters (500 feet) of sapphire fiber was coated with the Mo-O-C coating. This length of fiber consisted of Samples 195-60, 195-61, and 195-62. These production runs were made using a single fiber, and each required 6 to 7 hours of processing time. Representative sections of the coated fiber are shown in Figures 14 and 15. These figures show the approximately 4-μm thick Mo-O-C coatings at the beginning and end of Sample 195-62. These samples have small regions were the coating has spalled away from the fiber when it was cut for examination in the SEM. These Mo-O-C-coated fibers were heat treated in one atmosphere of flowing hydrogen at 1273K, while passing through the reactor at approximately 0.5 meters-per-minute (1.5 feet-per-minute). This conversion process produced

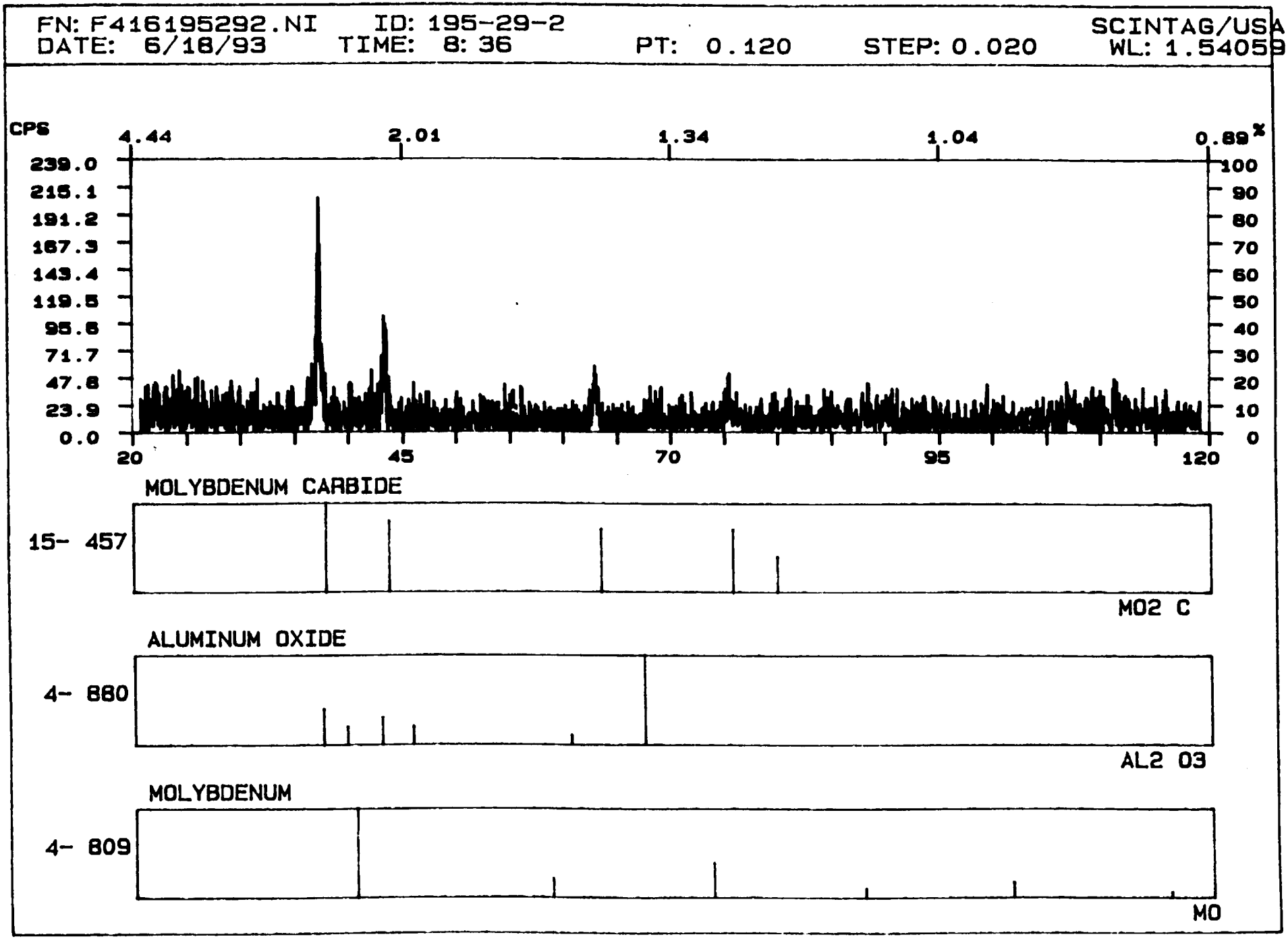
FN: F416195292.NI
ID: 195-29-2
SCINTAG/USA
DATE: 6/18/93
TIME: 8:36
PT: 0.120
STEP: 0.020
WL: 1.54059
CPS
4.44
2.01
1.34
1.04
0.89
X
239.0
215.1
191.2
167.3
143.4
119.5
95.6
71.7
47.8
23.9
0.0
100
90
80
70
60
50
40
30
20
10
0
20
45
70
95
120
MOLYBDENUM CARBIDE
15- 457
M02 C
ALUMINUM OXIDE
4- 880
AL2 03
MOLYBDENUM
4- 809
MO

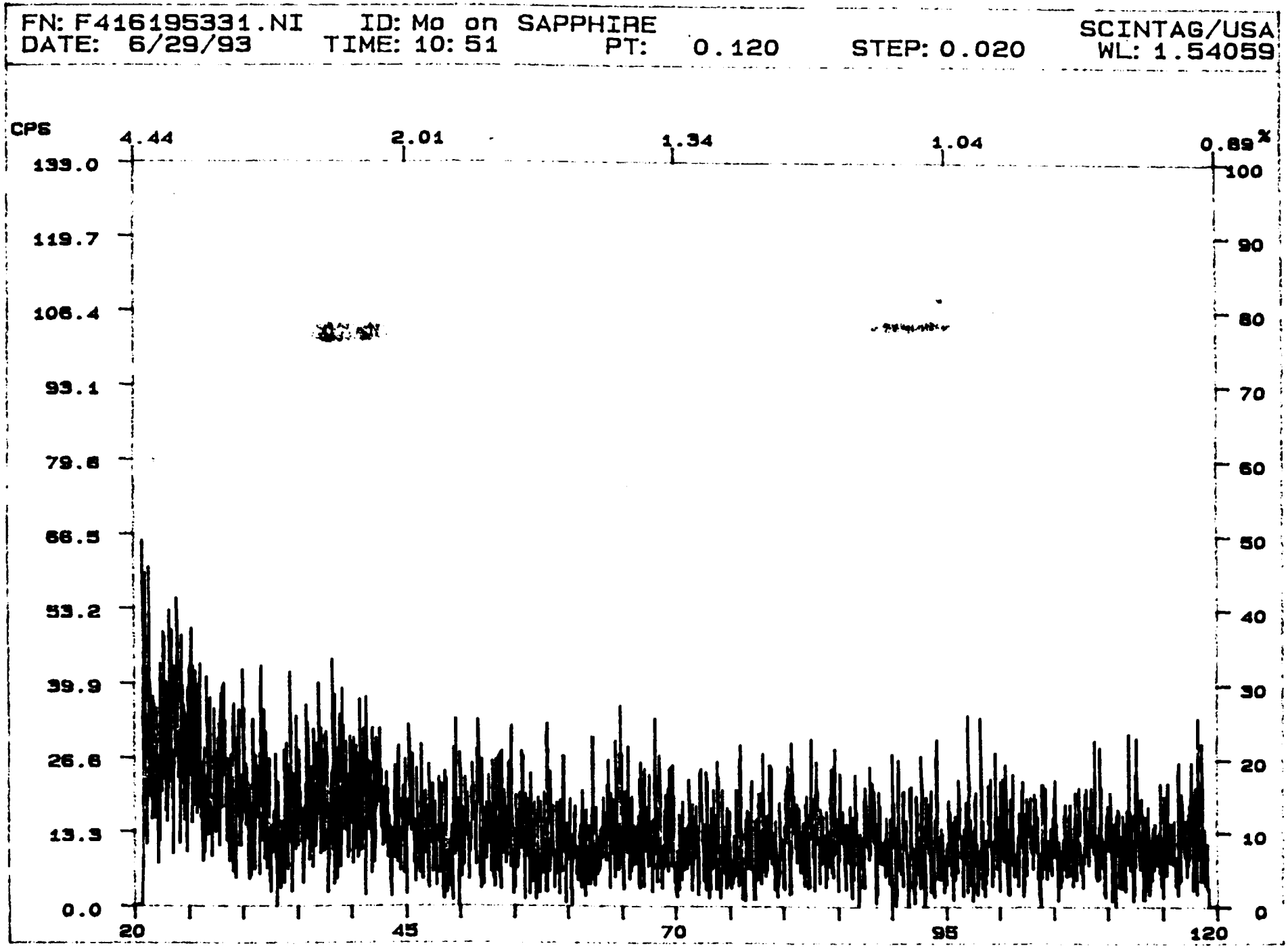

Figure 10. XRD Analysis of Sample 195-33-1 Produced at 6731

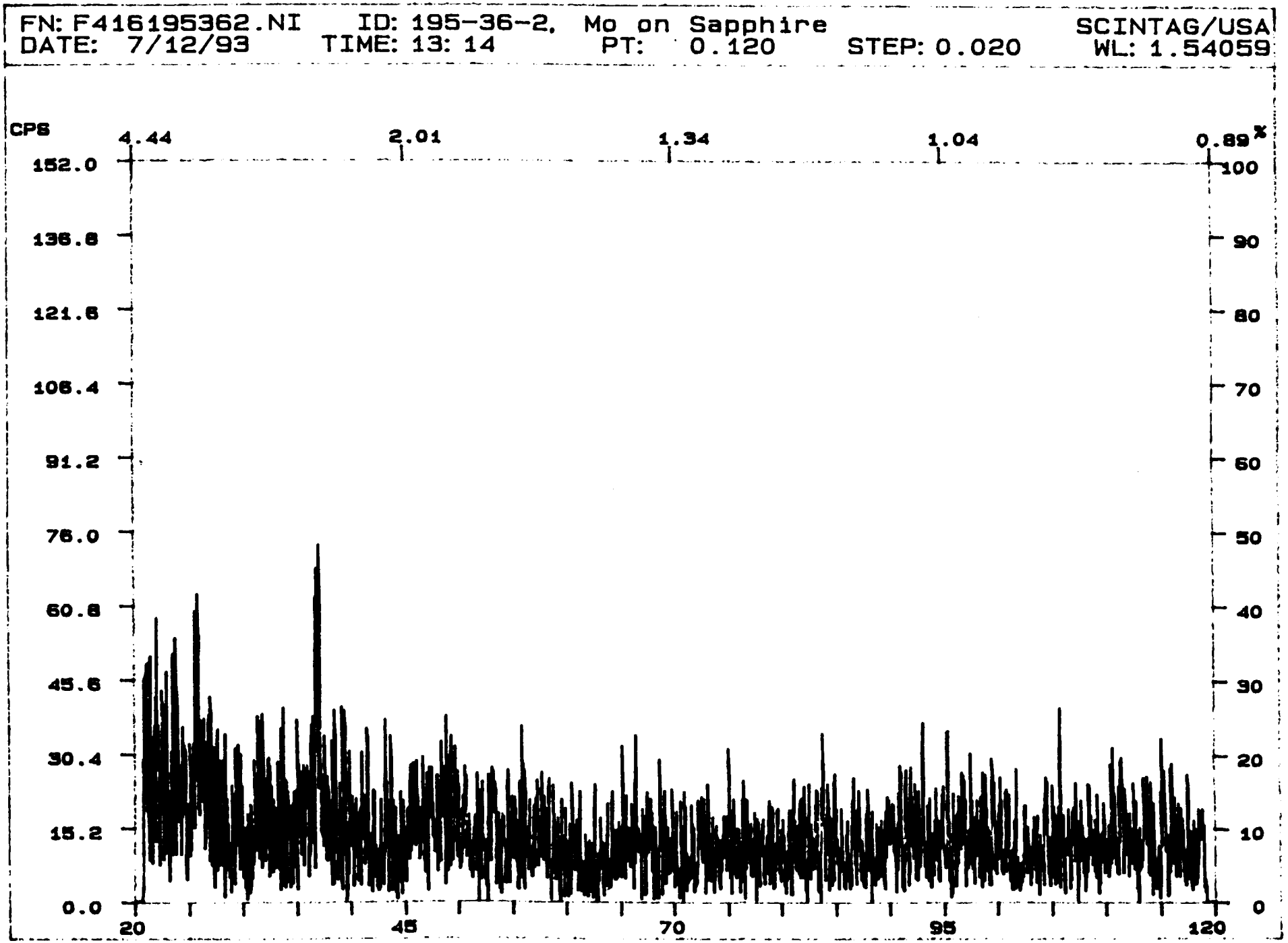

Figure 11. XRD of

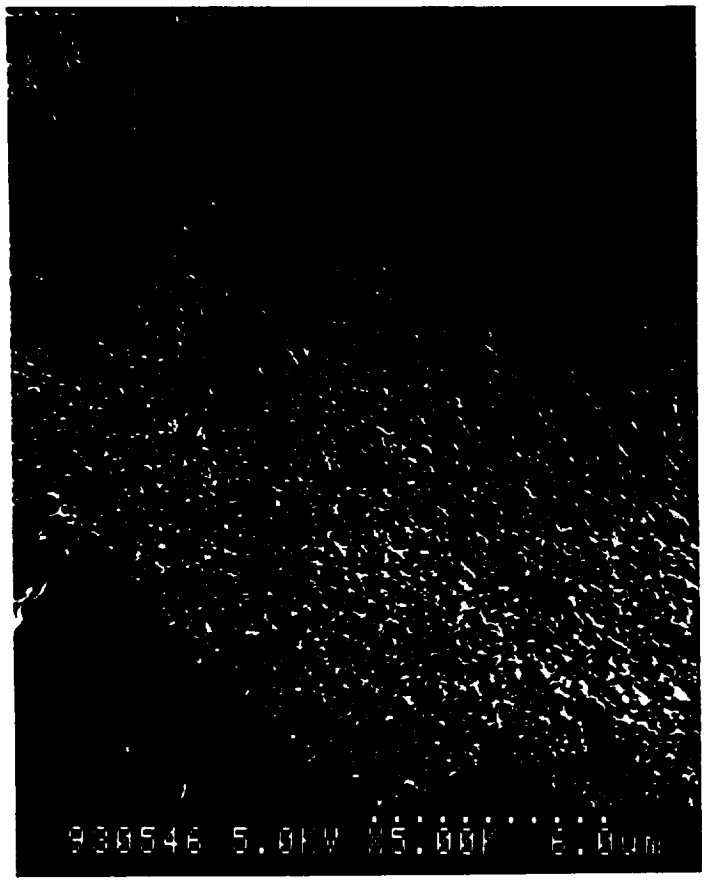

Figure 12. Morphology of Sample 195-36-2 After Heat Treatment

adherent molybdenum coatings with some residual porosity due to the volume reduction in the coating. The resulting coating was approximately 3-μm thick.

The results of the 3-μm coating runs indicated that producing the 5-μm coating in a single pass would be impractical with the current processing conditions. As a result, it was decided to produce the 5-μm coating in two passes, with the first Mo-O-C layer being reduced to Mo before applying the second layer. This approach was used to avoid generating large strains in the coating, which were thought to result from the volume decrease associated with the conversion to Mo. The first layer was produced in Run 195-74, and stet shown in Figures 16 and 17. The surface morphology of the coating (Figure 16) was moderately smooth, except for localized-powdery regions, which indicates some gas-phase nucleation. A cross-section of the coating (Figure 17) revealed that the coating was highly columnar and not fully dense, with a thickness ranging from approximately 1 μm to 3 μm.

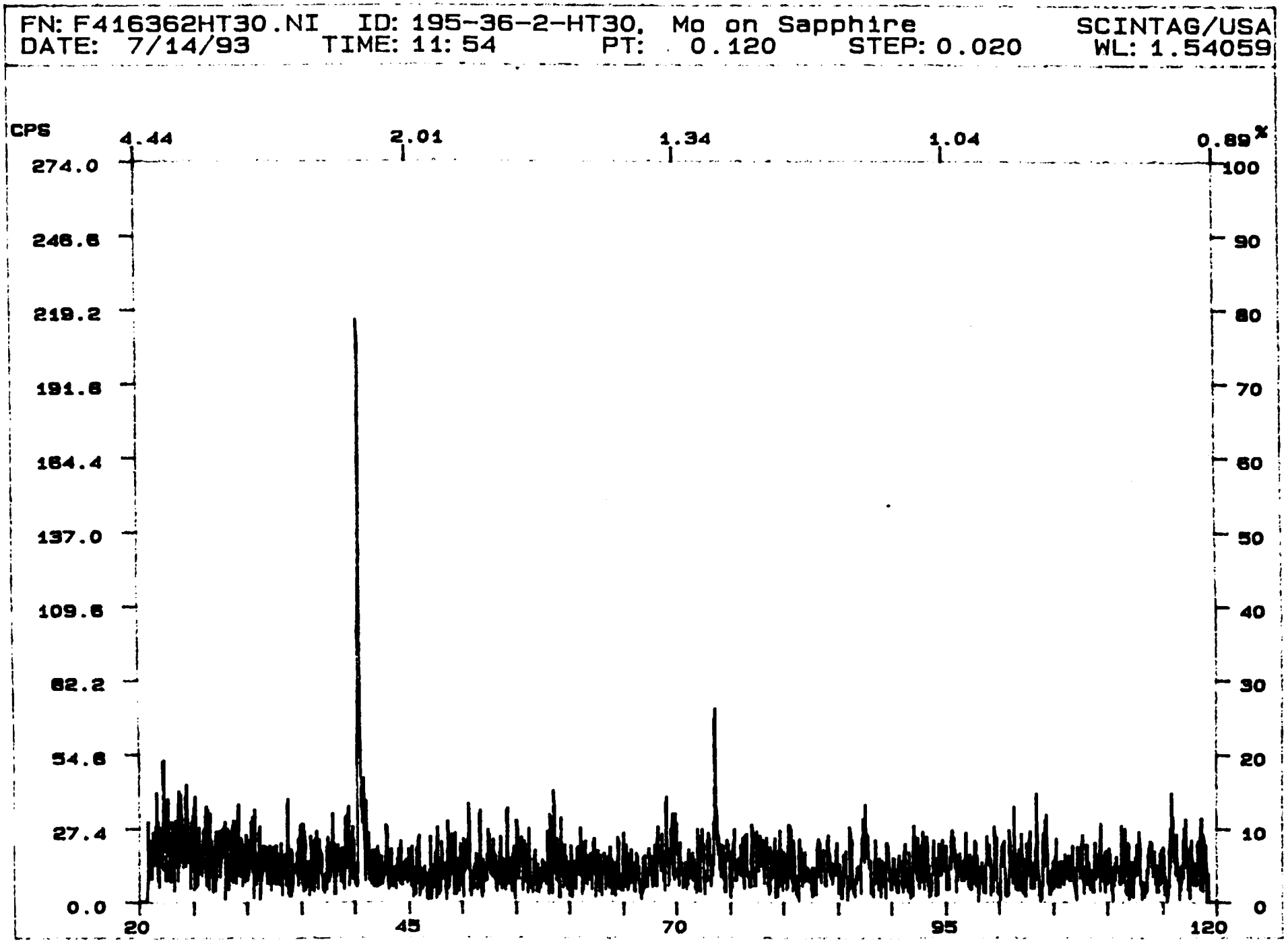

Figure 13. XRD Analysis of Sample 195-36-2 After Heat Treatment

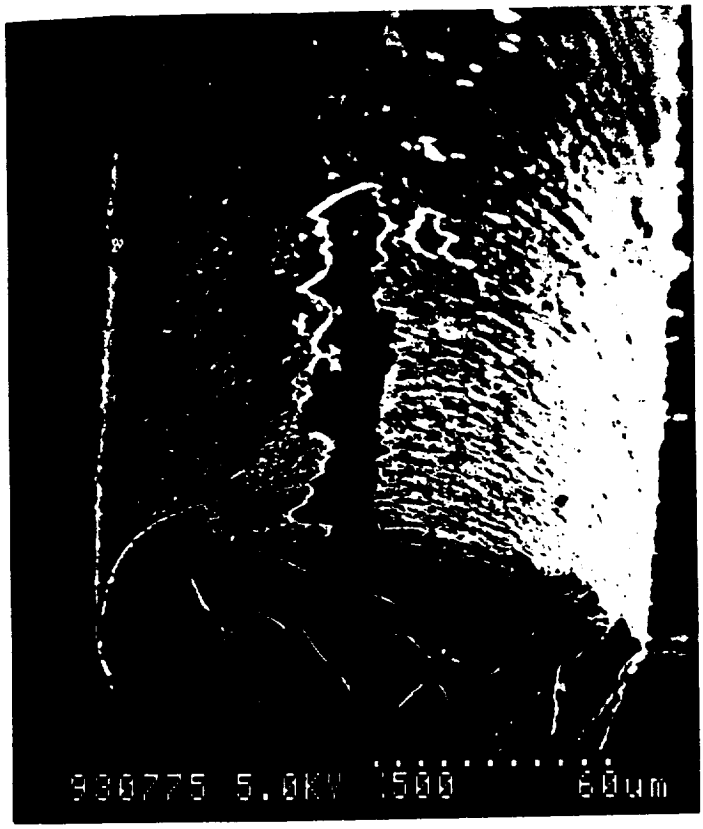

Figure 14. Sample 195-62-3 with 4 μm Mo-O-C from Start of Run

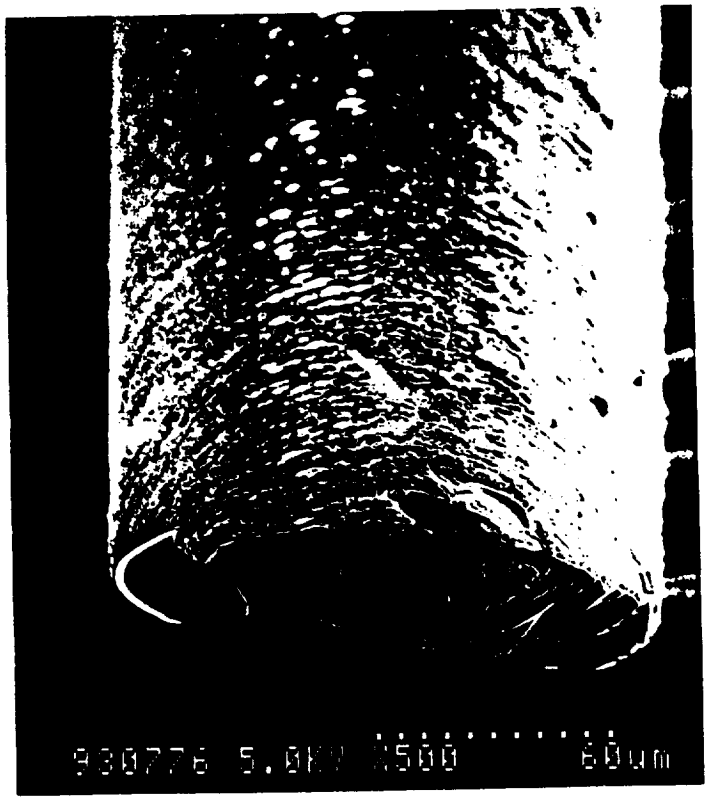

Figure 15. Sample 195-92-4 with 4 μm Mo-O-C from end of Run

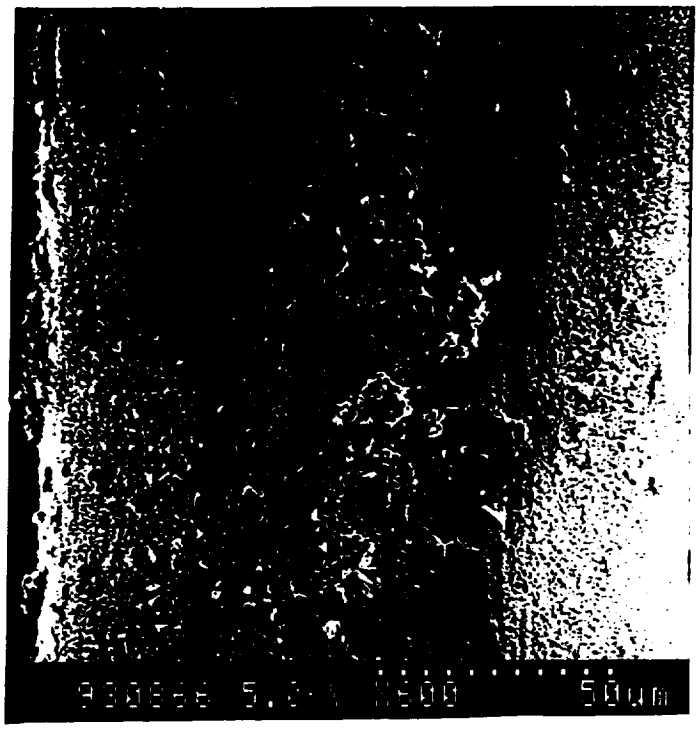

Figure 16. Morphology of Sample 195-74

Figure 17. Columnar Structure of Sample 195-74

After heat treatment, the coating of Run 195-77 appeared to be nearly dense and was 1.5-μm to 2-μm thick. The second Mo-O-C layer was deposited onto this heat-treated coating Run 195-79 to increase the coating thickness to 5 μm. The coating morphology and thickness changed significantly during this run. Figure 18 shows the initial section of the coating, which had a thickness of only a few microns, while the latter section of fiber had a very thick and non-uniform coating (Figure 19). The end of the fiber had local- coating thicknesses of 15 μm to 20 μm which appeared to be columnar and not fully dense. The second layer of Mo-O-C was heat-treated in Run 195-80, and an examination of the coating indicated a dendritic morphology (Figure 20) which had pulled away from the fiber fracture surface (Figure 21). Closer examination of this coating (Figure 22) showed that the first Mo layer appeared to be nearly dense, but the second pass produced a dendritic coating with significant porosity. The poor quality of this coating was disappointing, but this fiber was sent to NASA for testing and evaluation.

The poor results for the 5-μm coatings refocused our efforts onto demonstrating a higher-deposition rate which would produce a better quality coating for the production of the 10-μm coating. In making the next test run (Sample 257-9), a remarkable change in coating rate and structure was achieved by eliminating the 0.5 SLPM of Ar used to dilute the gases exiting from the sublimator and by slowing the fiber speed from 0.5 meters-per-minute (1.5 feet-per-minute) to 0.25 meters-per-minute (0.8 feet-per-minute). By eliminating the 0.5 SLPM of Ar, the system pressure dropped from 335 Pa (2.5 torr) to 133 Pa (1.0 torr), but all other parameters for Runs 257-9 and 195-79 were the same.

Figures 23 and 24 show the coating from the center of the 82 meter (270 foot) test run fiber. The coating in these micrographs is approximately 7-μm thick and has a columnar structure. The coating is relatively smooth (Figure 23) and appears nearly dense (Figure 24). Figures 25 and 26 show the morphology and texture of the 20mm Mo-O-C coating produced at the end of the run.

Figure 18. Start of Second Layer for 5 μm Mo Coating

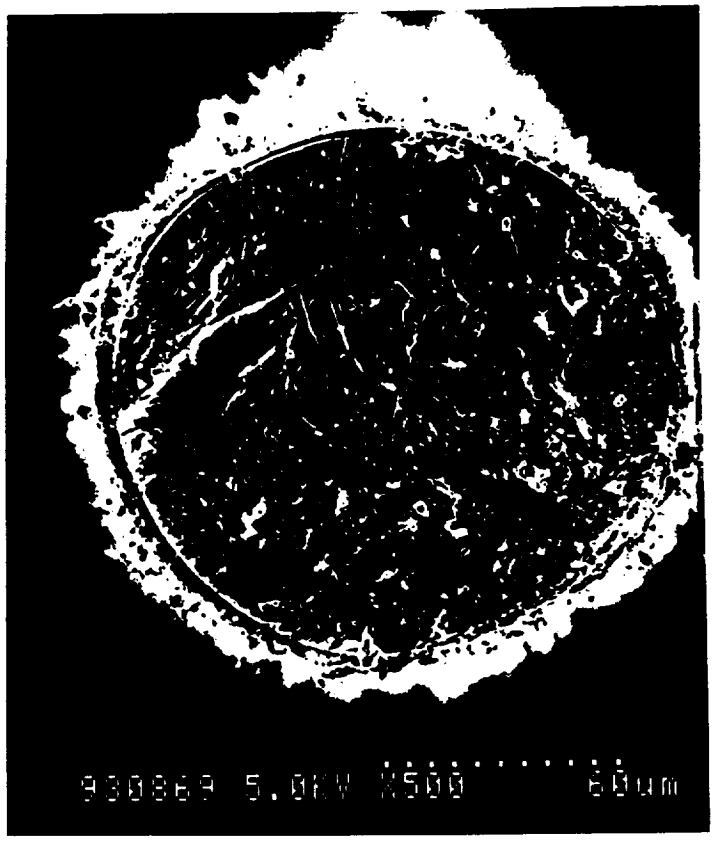

Figure 19. End of Second Layer for 5 μm Mo Coating

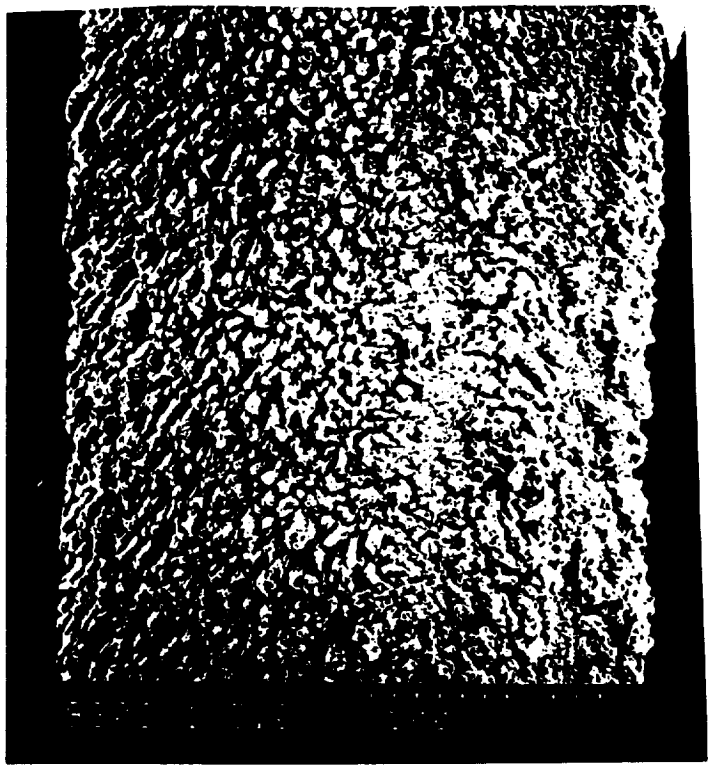

Figure 20. Heat-Treated Mo Coating With Dendritic Structure

Figure 21. 5 μm Mo Coating Debonded from Fiber

Figure 22. Columnar Growth and Porosity in 5 μm Mo Coating

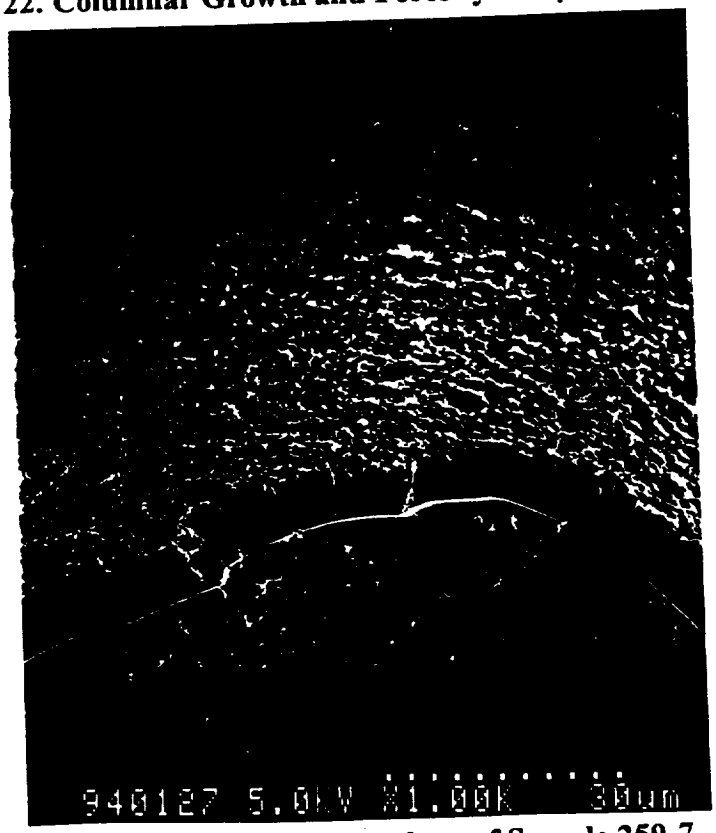

Figure 23. Smooth Morphology of Sample 259-7

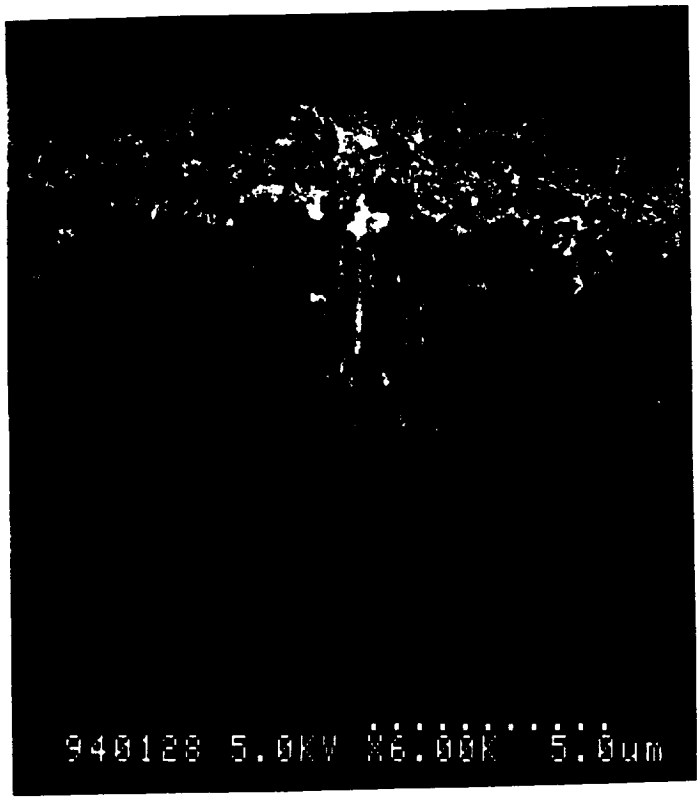

Figure 24. Dense and Columnar Structure of Sample 259-7

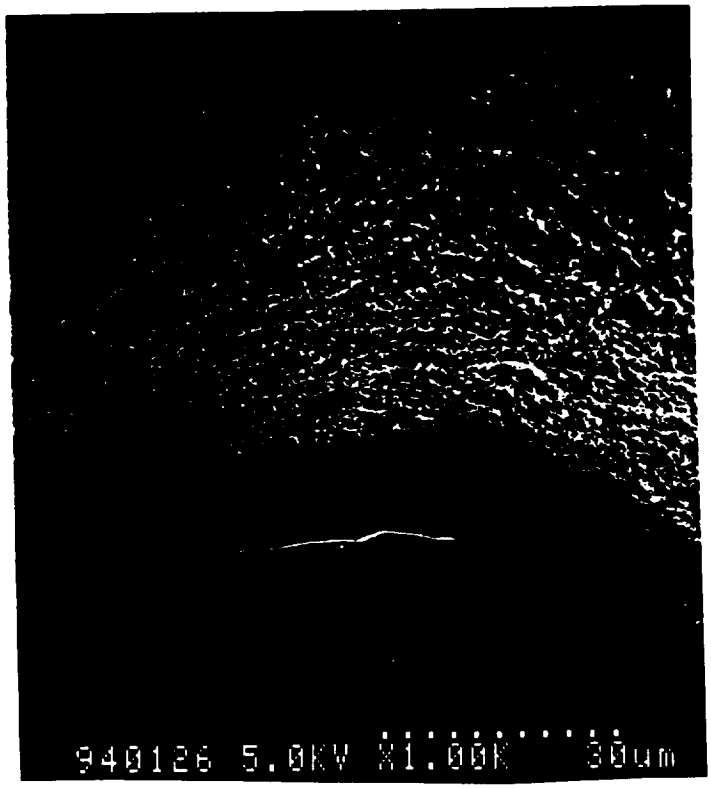

Figure 25. 20 μm Coating from Sample 257-9

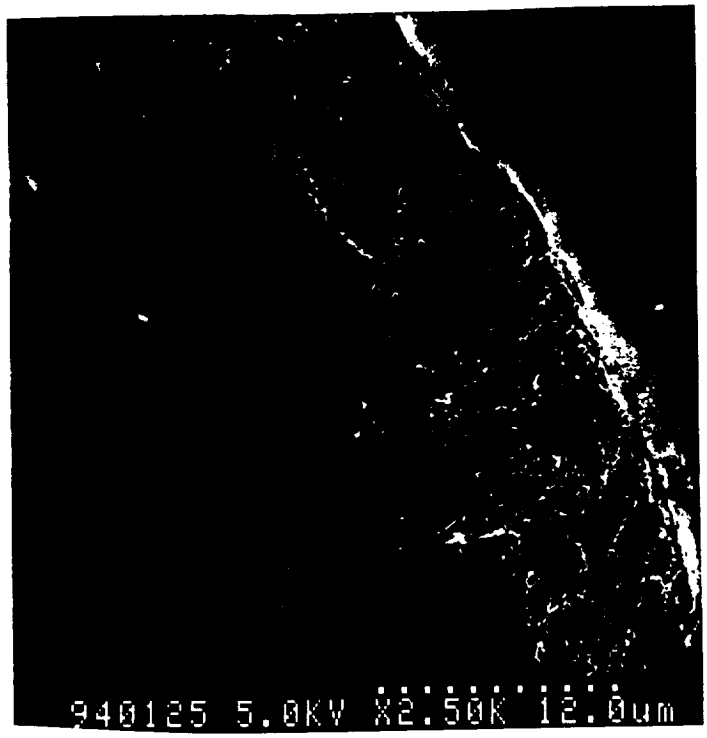

Figure 26. Growth Structure of 20 μm Mo-O-C Coating

The only observed difference in processing parameters between the middle and end sections of the fiber was a change in the sublimator pressure from 27 Pa to 67 Pa (0.2 torr to 0.5 torr).

At this time a series of equipment problems resulted in a long delay between coating runs. Once these problems were corrected, Run 257-20 produced a 12-μm thick Mo-O-C coating shown in Figure 27. The coating was applied at a temperature of 773K, a pressure of less than 133 Pa (1 Torr), and a speed of approximately 0.2 meters-per-minute. The coating appears relatively smooth and columnar, but it had only moderate adhesion to the fiber, since it exhibited some spalling at the fracture surface. This coated fiber was heat treated in one atmosphere of flowing hydrogen at 1373K, using a fiber speed of 0.2 meters-per-minute, to convert the Mo-O-C coating to molybdenum. The reduced coating is shown in Figures 28 and 29. Figure 28 shows the coating uniformity and improved adhesion to the fiber, as well as the porosity of the coating. The high degree of porosity in the coating is even more obvious in Figure 29, which shows the individual columns of Mo, approximately 15-μm in length, attached to the fiber surface.

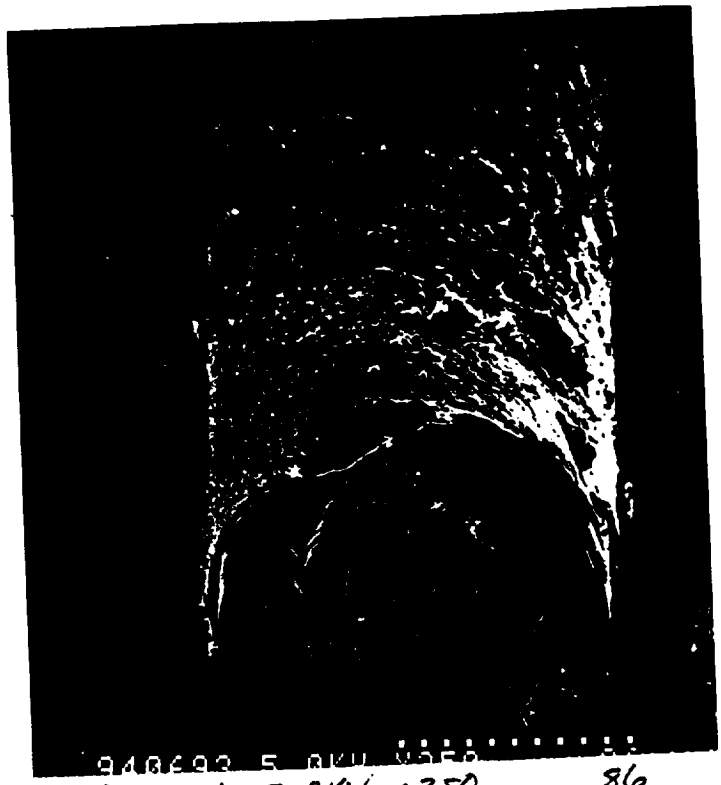

Figure 27. 12 µm Coating from Sample 257-20

Figure 28. Porous and Adherent Mo on Sapphire

Figure 29. Porosity in 10 μm Mo Sample

As with the thinner coatings, the volume reduction in the thicker coating, as it is reduced from Mo-O-C to Mo, is significant; and the reactors could not be brought to a temperature high enough to produce sintering of the Mo. This fiber was also delivered to NASA for testing and evaluation.

With the demonstration of these improved deposition conditions, another lot of fiber, approximately 70-meters-long, with a 5 μm coating, was produced. The Mo-O-C coating from this Run 257-24 (Figure 30) was less columnar than previous coatings and appeared to be approximately 7-μm-thick. This coating was heat treated, as described previously, but had a markedly different morphology after processing. The coating was very smooth (Figure 31), appeared to be nearly dense, and had a thickness of approximately 3 μm. The coating is difficult to see in the micrographs, but the metallic-silver color of the Mo coating was readily visible on the entire length of fiber. This sample of fiber was also delivered to NASA for testing and evaluation.

Figure 30. Mo-O-C for Second Lot of 5 µm Coating

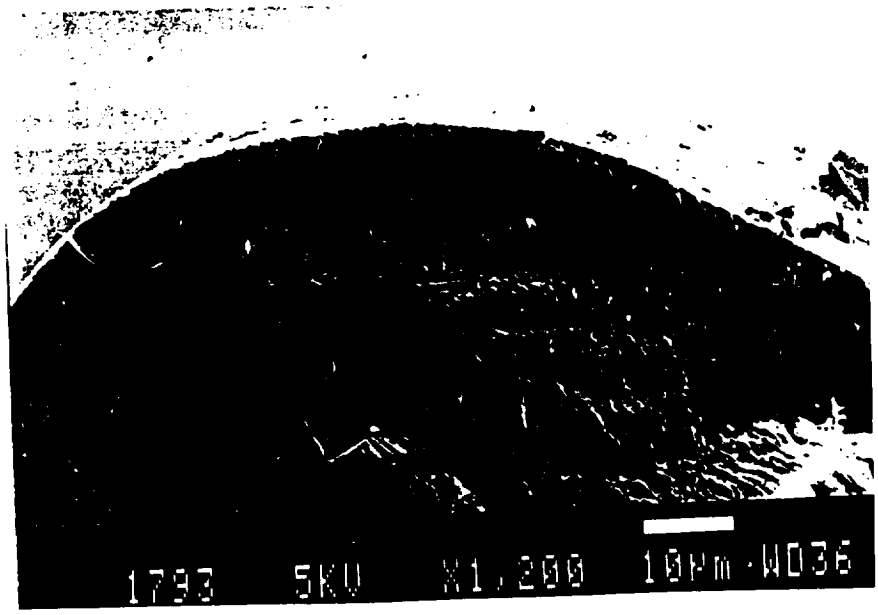

Figure 31. Heat Treated Coating

3.2 CVD Functionally Gradient Material

3.2.1 Reactor Design and Installation

A major part of the FGM Task was the design and assembly of a continuous-fiber coating reactor with a flexible delivery system for controlling the precursor distribution throughout the coating volume. This reactor was also equipped with scrubbing and precursor-handling systems adapted for working with volatile nickel compounds. The reactor was installed inside a walk-in hood, which was kept at a reduced pressure compared to the rest of the lab. A schematic of the reactor is provided in Figure 32. The reactor utilized an Inconel 600 retort, which was heated by a three-zone resistance furnace. The fiber-winding system was installed in differentially pumped chambers to protect both the drive system and the fiber from contamination by the reactant streams. Two precursor-delivery lines entered through the top of the retort, and each ran the length of the reactor. Each delivery line had a series of holes to tailor the distribution of the

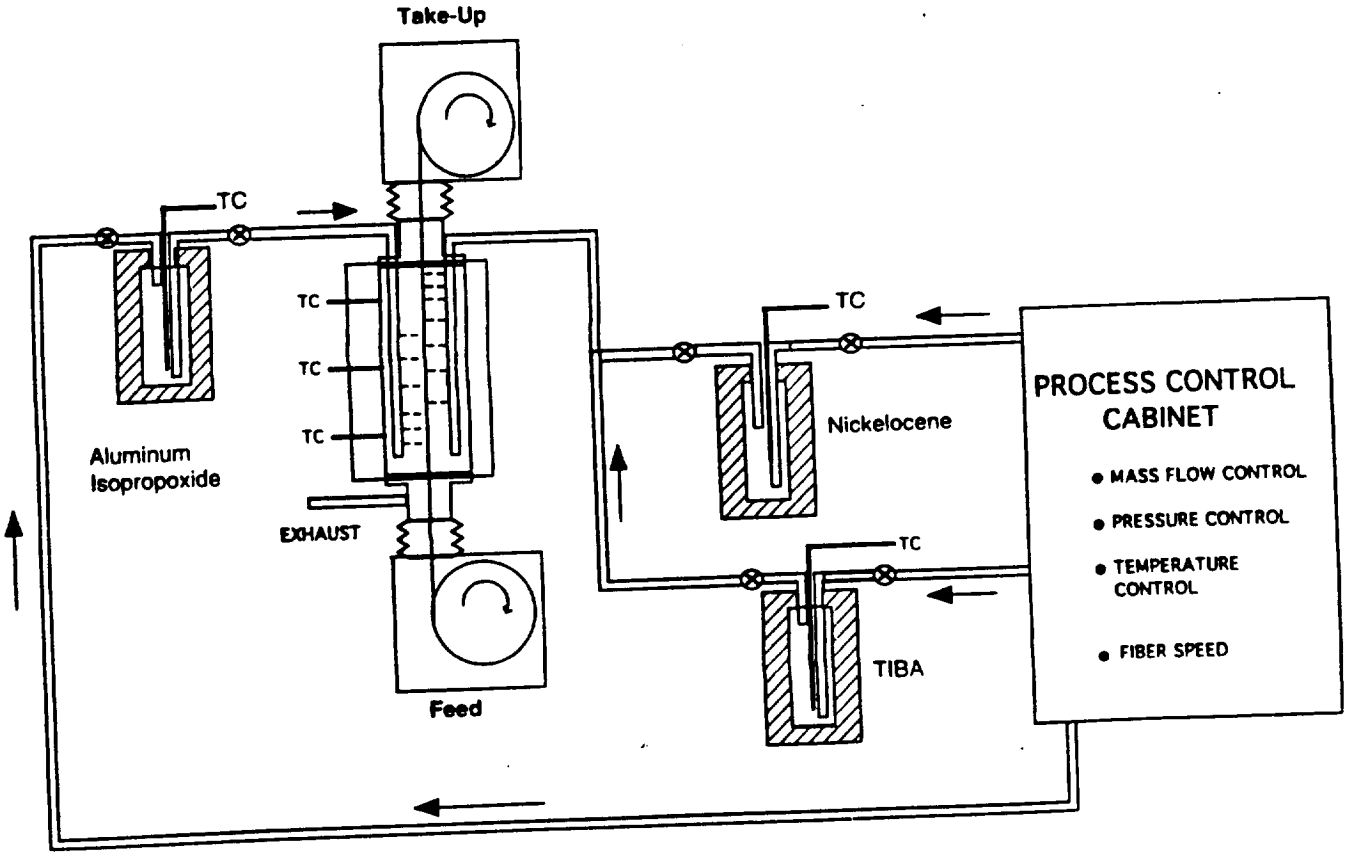

Figure 32. FGM Reactor Schematic

precursors in the reactor. To produce the homogeneous layers on each side of the coating, the fiber entered and exited the reactor through small tubes into which the precursors for either NiAl or alumina were added. This precursor-delivery system was added to produce the FGM coating, which needed an alumina layer adjacent to the sapphire fiber, an NiAl layer on the exterior of the coating, and a smooth transition between the homogeneous layers. Each zone of the furnace was independently controlled using a Eurotherm programmable controller, and MKS process-control equipment was used for gas-flow and pressure control. The bubbler and sublimator temperatures for the precursors were controlled using Omega CN9000 series controllers. All of the gases were exhausted from the bottom of the reactor. The exhaust system consisted of a liquid-ring pump and a venturi to draw the gases through the scrubbing system. The liquid-ring pump was filled with an aqueous solution to neutralize any unreacted nickelocene.

3.2.2 CVD Alumina

With the deposition temperature range for NiAl expected to be 573K to 773K, aluminum isopropoxide was selected as the alumina precursor because of its ability to deposit alumina at similar temperatures. Aluminum isoproxide was melted in a bubbler and transported to the reactor using argon as the carrier gas. Hydrogen was mixed with the gas stream from the bubbler, at a H_2:Al ratio of between 5 and 20. This was done to suppress any decomposition of the hydrocarbon by-products from the reaction. In a conventional process, excess oxygen, or water vapor could be added to prevent carbon deposition, but excess oxygen would make the co-deposition of NiAl difficult. Process development was carried out in a series of semi-continuous and short continuous runs. In a semi-continuous test, a section of fiber was held stationary in the coating section for between 5 and 10 minutes, then the process gases were shunted around the reactor and the fiber moved out of the reactor. Using this technique, up to 12 parameter sets were screened in one "run".

The first set of experiments (195-08,-10, and -12) used deposition temperatures between 723K and 773K and produced the "island" growth morphology seen in Figure 33. This figure shows discrete "islands" were the coating has been deposited and relatively large uncoated regions

between islands. This morphology is typical of low-precursor saturation and high- deposition temperature. For Sample 195-15-4, the deposition temperature was reduced to 573K, while the bubbler temperature was raised to 423K. These changes produced a continuous film with a faceted morphology. A 30-minute continuous run was performed at a temperature of 573K and the carrier gas flow through the sublimator was doubled to increase the transport of the aluminum isopropoxide to the reactor. The alumina-coated fiber produced in this run was somewhat smoother and appeared to have a continuous coating. Closer examination of the fiber showed a coating between 1-μm and 4-μm thick, with the majority being closer to 1 μm, which was adherent to the fiber. Sample 195-18 was produced using the same conditions, and Figures 34 and 35 show a typical section of this sample. The coating is somewhat smoother than previous samples, but it still has a moderate texture. The coating is adherent to the sapphire fiber, and it appears to be approximately 0.5-μm thick. This sample was provided to NASA-LeRC for evaluation of the effect of a polycrystalline alumina coating on the mechanical properties of the sapphire fiber.

Figure 33. $Al_2O_3$with Island Growth Morphology

Figure 34. Al_2O_3-Coated Sapphire Fiber

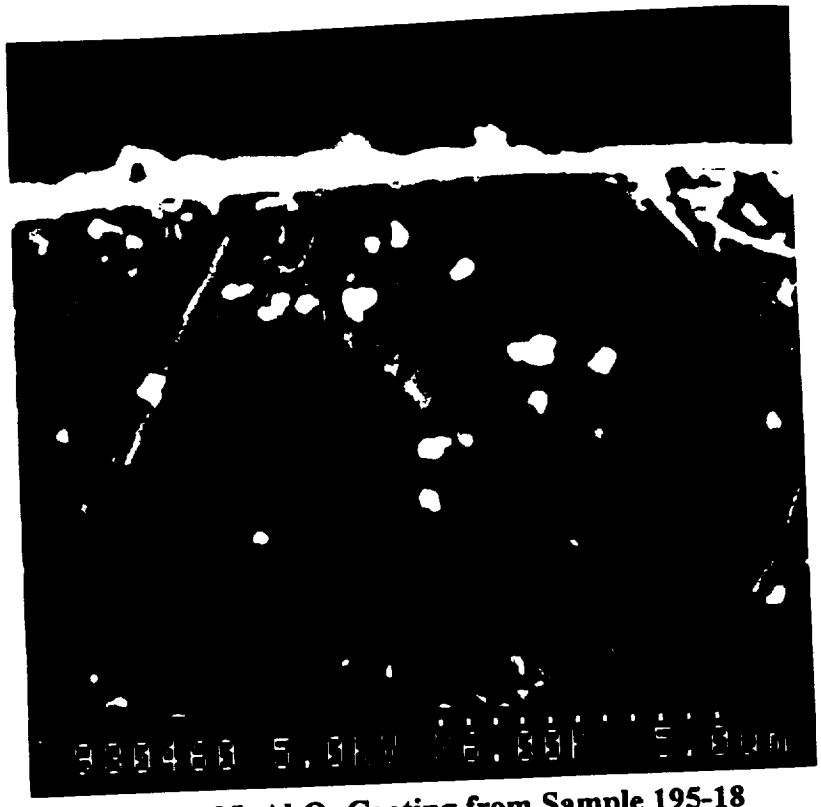

Figure 35. Al_2O_3 Coating from Sample 195-18

3.2.3 CVD NiAl and FGM

As mentioned previously, nickelocene ($Ni(C_5H_5)_2$ or bicyclopentadienyl nickel) and tri-isobutyl aluminum (TIBA) were selected as precursors for NiAl. Nickelocene is a solid at room temperature with a vapor pressure of less than 13 Pa (0.1 torr) at 298K. This slowly increases to approximately 266 Pa (2 torr) at 373K. TIBA is a liquid at room temperature which has a vapor pressure of 58 Pa (0.4 torr) at 298K and 2.7 KPa (20 torr) at 373K. Once the reactor had been assembled and leak tested, transport efficiency tests were conducted for both precursors. The nickelocene powder was loaded into a stainless steel cylinder, installed onto the reactor, and heated to 423K. During the 45-minute test, a/H_2 carrier-gas flow of 1 SLPM was used to transport the nickelocence at a sublimator pressure of 8 KPa (60 torr). By weighing the sublimator before and after this test, and knowing the carrier gas flow, temperature, and sublimitor pressurer transport efficiency of just over 20 percent was calculated for the nickeloncene. A similar experiment for the TIBA, using a H_2 carrier-gas flow of 1 SLPM, a bubbler temperature of 323K, and a pressure of 23.3 KPa, yeilded a transport efficiency of approximately 95 percent. The dramatic difference in efficiencies for the two precursors is likely due to poor contact, or channeling, of the carrier gas in the nickelocene powder.

The first deposition test for NiAl was a 18-minute static test with each of the three zones of the furnace at a different temperature. The goal of this test was to determine an initial temperature for process development. Thermodynamic modeling had shown that the reaction should have been possible at temperatures as low as 473K. All of the precursor gases were introduced at the top of the reactor, and the furnace zones were set for 523K, 623K, and 723K from top to bottom, respectively. Five samples were taken from this test (195-68-1 through -5) and characterized by SEM and semi-quantitative EDS. Sample 195-68-1 was within the 523K section, while 195-68-5 was at 723K. Sample 195-68-1 (Figure 36) was at least 100-μm thick, but was very rough and hard with numerous cracks. Semi-quantitative EDS analysis showed that it contained approximately 88 atomic percent (a/o) Al and 12 a/o Ni.

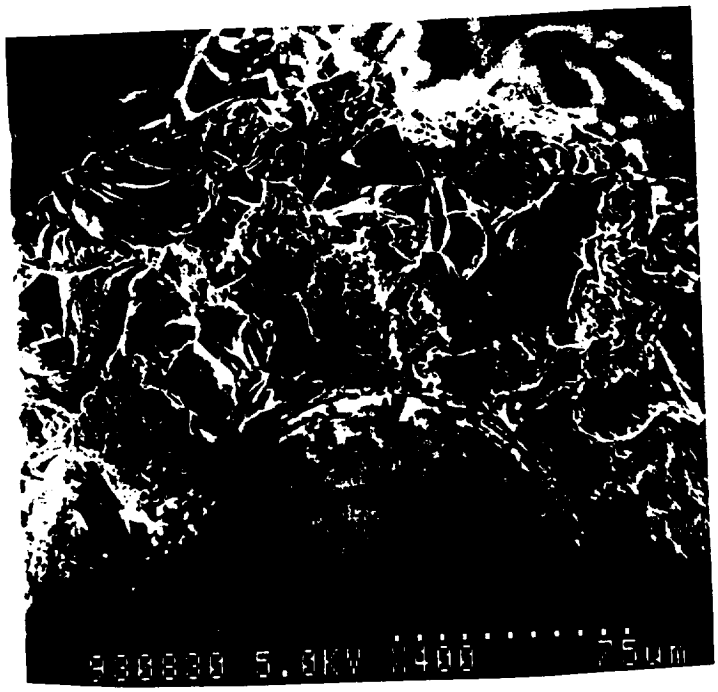

Figure 36. Sample 195-68-1 Produced at 523 K

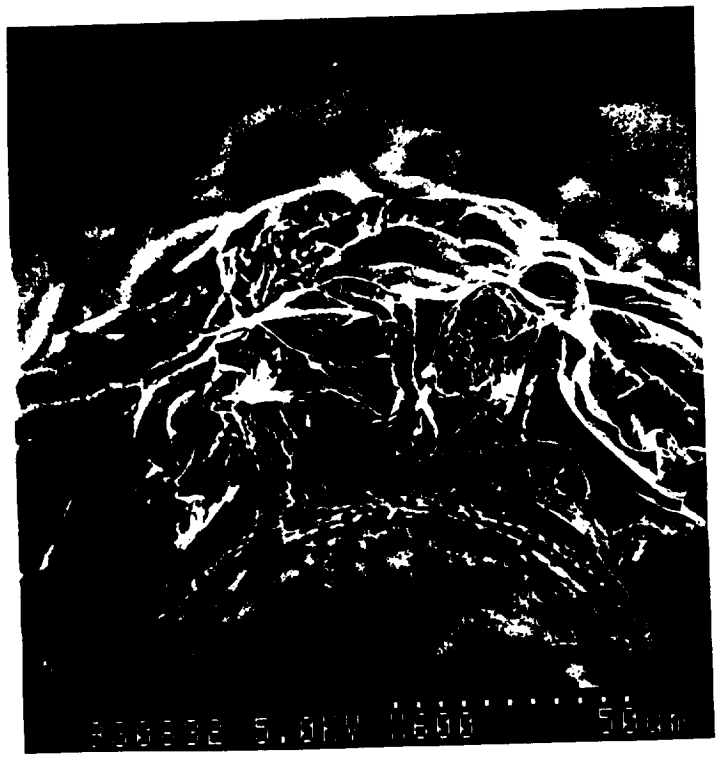

Figure 37. Sample 195-68-2 with 76 a/o Al and 24 a/o Ni

Sample 195-68-2 (Figure 37) was taken from the fiber at the transition between the 523K and 623K sections. This coating was also very rough and contained many surface cracks. It was approximately 40-μm thick and contained approximately 76 a/o Al and 24 a/o Ni. Sample 195-68-3 (Figure 38) was taken from the fiber approximately 3 inches into the 623K zone. The coating was generally smoother than the first two samples, but it still contained numerous cracks and large growth nodules. The coating was approximately 20-μm thick and consisted of approximately 70 a/o Al and 30 a/o Ni. The coating in Sample 195-68-4 (Figure 39) was substantially more uniform than those from the previous regions, but it had a uniform dispersion of small nodules on the surface and was 15-μm thick. This sample contained approximately 83 a/o Al and 17 a/o Ni. The last sample from the fiber, 195-68-5 (Figure 40), was selected from the middle of the 723K section. The coating contained approximately 70 a/o Al and 30 a/o Ni, was only 7-μm to 10-μm thick, and exhibited widly dispersed growth cones.

The thermal-gradient test revealed that the highest deposition rates were achieved at the lower temperatures, while higher nickel contents were obtained above 623K. These results were expected, since TIBA can be used to deposit Al at temperatures as low as 423K, and it would be expected to deposit readily at the lower temperatures used in this trial. Also as the concentration of TIBA decreased along the length of the reactor, less Al was deposited. This may have allowed the slower-reacting nickelocene to become a larger contributor to the coating. A series of isothermal experiments, which attempted to balance deposition rate (>1 μm per minute reached) with correct composition, was begun. The first of these isothermal experiments was 195-72, from which we examined four samples. As with 195-68, the thickest coating was produced nearest the precursor inlet, and thickness then decreased along the length of the reactor. During this 20 minute test at 548K, the upper section of the fiber had a rough and angular coating approximately 30-μm to 40-μm thick, while the bottom third of the fiber had a generally smooth coating which was 2-μm to 3-μm thick. The four spots (Samples 195-72-2, -3, -4, -5) along the fiber axis that were examined by EDS had the following respective compositions: 56 a/o Al and 44 a/o Ni, 74 a/o Al and 26 a/o Ni, 52 a/o Al and 48 a/o Ni, and 69 a/o Al and 31 a/o Ni.

Figure 38. Sample 195-68-3 Produced at 623 K

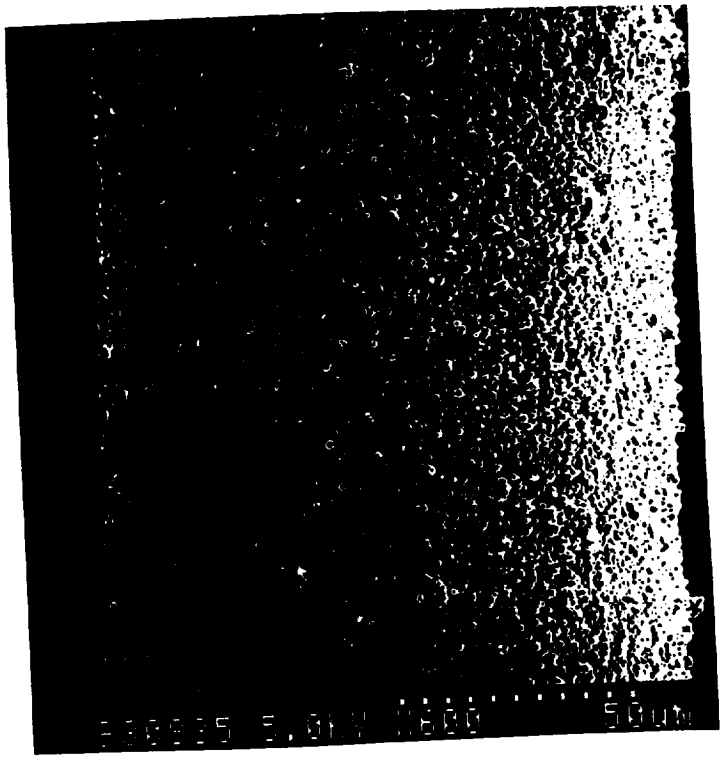

Figure 39. Sample 195-68-4 with 83 a/o Al and 17 a/o Ni

Figure 40. Sample 195-68-5 Produced at 723K

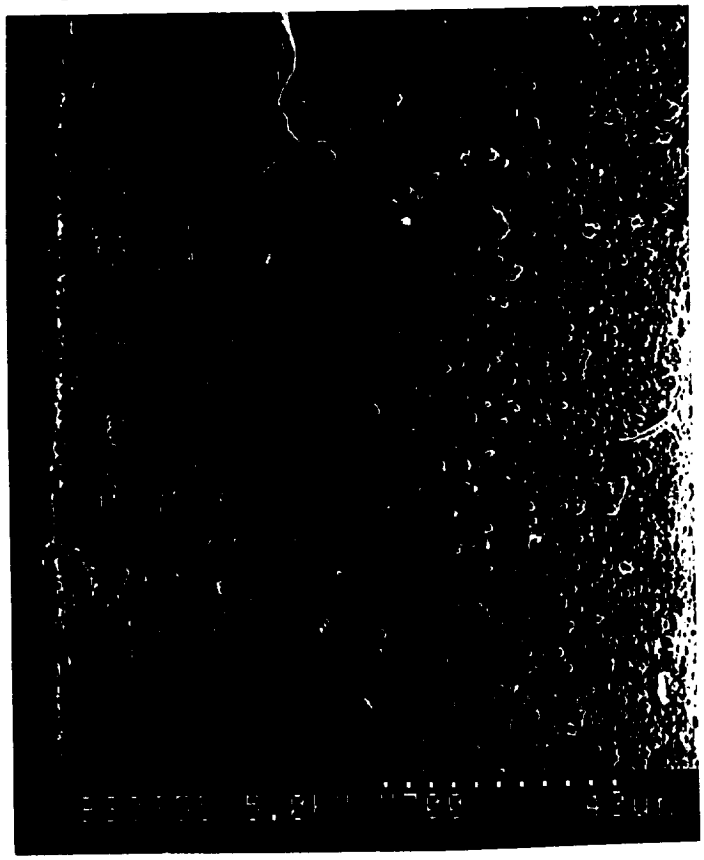

Figure 41. Sample 195-72-4 with 52 a/o Al and 48 a/o Ni

The coating from Sample 195-72-4, which had a nearly stoichiometric Ni:Al ratio, is shown in Figure 41. This coating is smooth (except for the surface nodules) adherent to fiber, and has a thickness of approximately 3-μm. A short static test (195-76) was performed at a reactor temperature of 673K. The carrier-gas flow rate through the nickelocene sublimator was increased to 2 SLPM to increase the nickel content of the coating. This test produced a coating between 2-μm and 3-μm thick (Figure 42) which was rough and did not appear to be fully dense. The composition of the coating was examined in several areas and displayed nickel contents of 20 a/o to 26 a/o. An XRD pattern was made from the as-deposited sample, and the results are shown in Figure 43. A listing of "peaks" and proposed phase identification is provided in Table 1. As can be seen, the intensity of the pattern is very low, but the coating was thick enough to prevent diffraction from the sapphire fiber. Phases that were identified from this pattern included, Al_3Ni, Al_3Ni_2, and Al. With the excess aluminum in the coating this distribution of phases would be expected. However this does provide evidence for the direct formation of crystalline aluminides at low temperature using this process.

Since a higher-deposition temperature and carrier-gas flow through the nickelocene did not increase the nickel content of the coating, the temperature was lowered to 623K to improve the coating morphology. In Sample 195-81, the carrier gas to the nickelocene was reduced to 0.6 SLPM to prevent clogging of the delivery system, and the TIBA transport rate was dramatically reduced (#'s). Analysis of the coating along the length of the fiber revealed that the first 15 centimeters had only 4 a/o nickel, while the balance contained between 11 a/o to 20 a/o. There was no apparent pattern to the distribution. The highest-quality coating, approximately 45 centimeters into the hot-zone, had only 11 a/o nickel and is shown in Figure 44. This section of the coating is approximately 0.5-μm to 1.0-μm thick with scattered protrusions from the surface. Several other sections of the fiber had cracks in the coating which produced a "dried mud" texture. This is typical of a coating with a high-residual tensile stress.

The inconsistent level of nickel in the coatings was apparently related to the transport of the nickelocene. Processing changes which would be expected to increase the nickel content of the

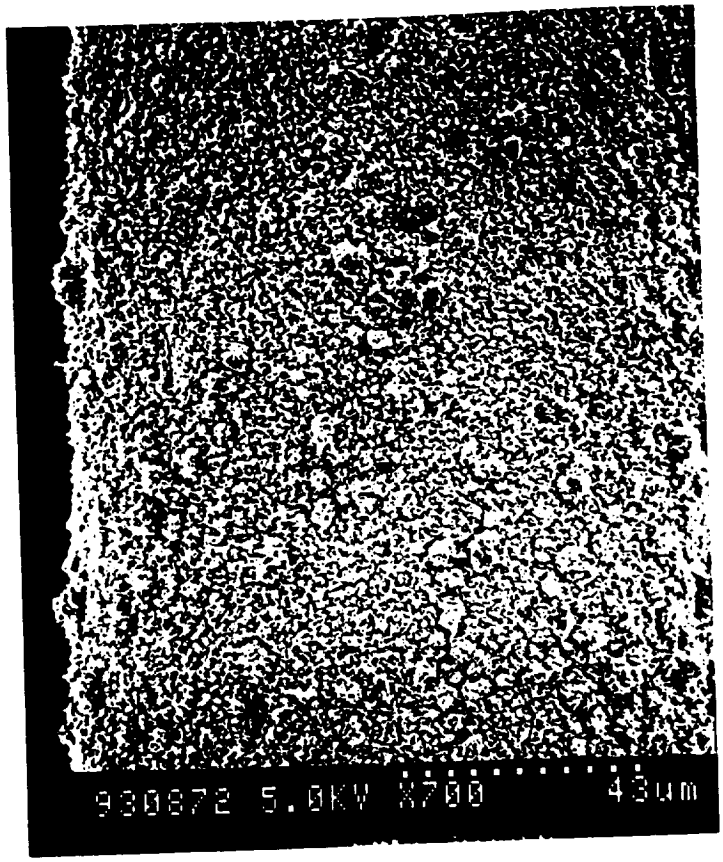

Figure 42. 2 μm to 3 μm Coating on Sample 195-76

Table 1. Phases Present in Sample 195-76

2 Theta	D	Phase
43.280	2.0888	Al_3Ni
49.492	1.8402	Al_3Ni
25.025	3.5554	Al_3Ni_2
71.300	1.3216	Al_3Ni_2
38.576	2.3320	Al
47.100	1.9279	Al_3Ni

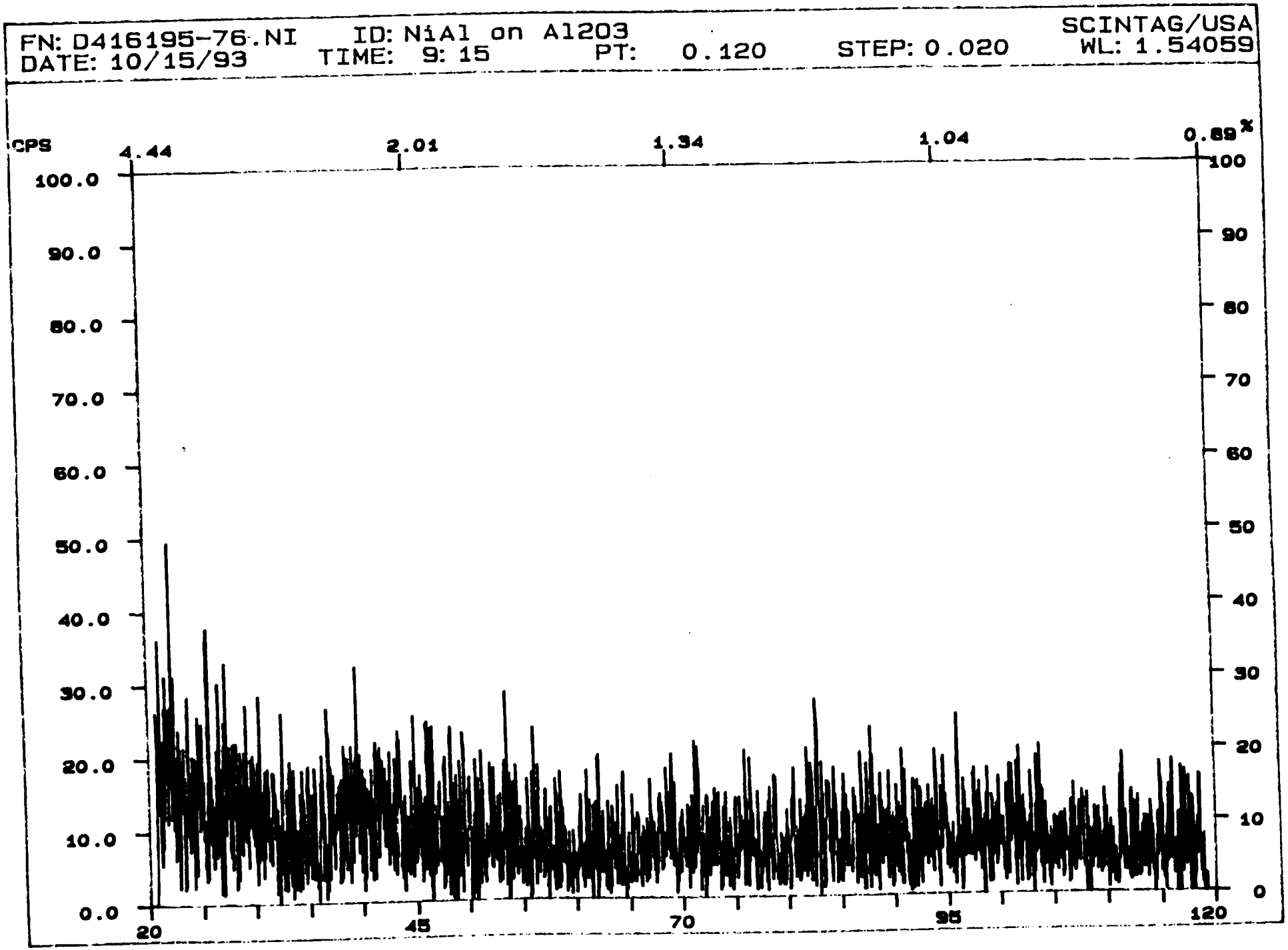
FN: D416195-76.NI
ID: NiAl on Al203
SCINTAG/USA
DATE: 10/15/93
TIME: 9:15
PT: 0.120
STEP: 0.020
WL: 1.54059
CPS
4.44
2.01
1.34
1.04
0.69
%
100.0
90.0
80.0
70.0
60.0
50.0
40.0
30.0
20.0
10.0
0.0
100
90
80
70
60
50
40
30
20
10
0
20
45
70
95
120

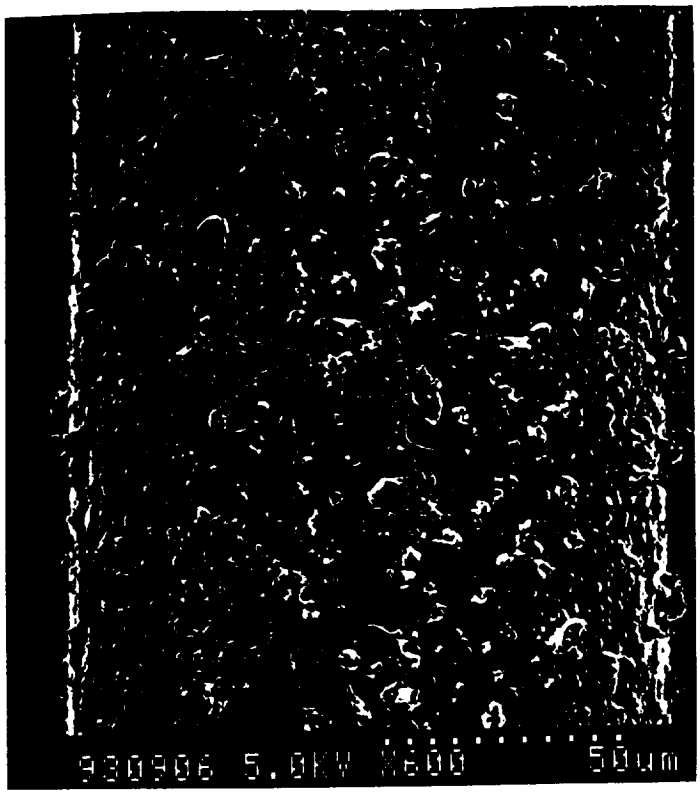

Figure 44. Sample 195-81 with 11 a/o Nickel

coating, such as an increased nickelocene carrier gas-flow rate and a higher-deposition temperature, had no predictable or repeatable effect.

Despite these difficulties, several runs were made to co-deposit NiAl and alumina. Sample 195-87 was produced by flowing argon through the aluminum isopropoxide bubbler for 4 minutes, then flowing all of the precursors for 8 minutes, and ending with the nickelocene and TIBA flows for approximately 6 minutes. A deposition temperature of 573K and a pressure of 8 KPa (60 torr) were used in this experiment. The coating produced in this run is shown in Figure 45, with the sample taken from the middle of the fiber. The coating is columnar and did not appear to be continuous. Analysis of the coating surface using EDS did not show the presence of nickel.

Throughout the FGM effort, nickelocene transport was an ongoing problem. The transport rate varied significantly between experiments. This made a difficult technical task even more complex and decreased the probability of success. After discussions with NASA, it was decided to drop the FGM coating development and substitute batch coating of sapphire fiber with CVD nickel.

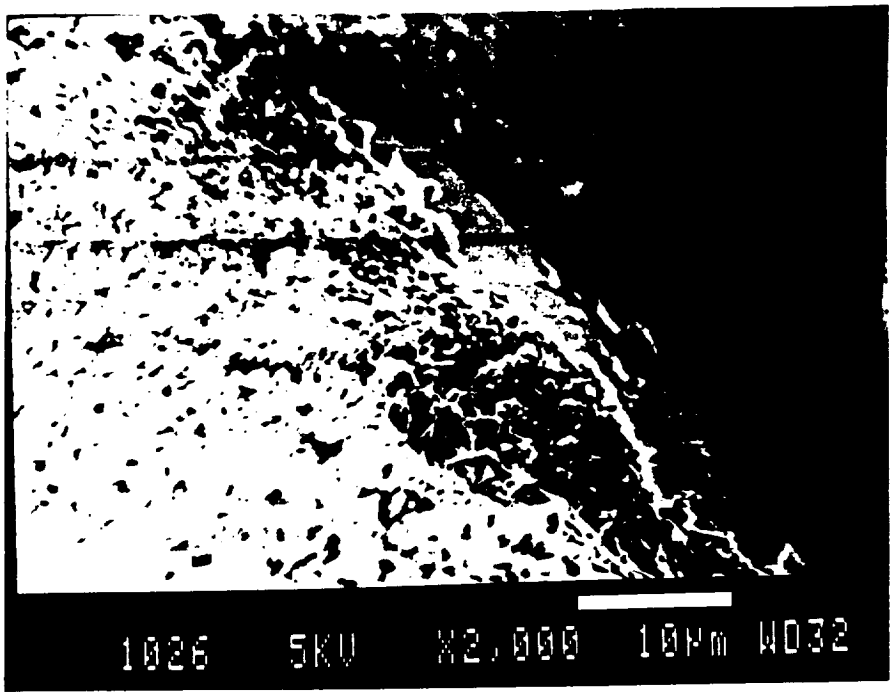

Figure 45. Coating Produced in FGM Sample 195-87

Since nickel has a CTE higher than either NiAl or sapphire, it may act as a compensating layer in this system. To prevent reaction between the nickel and NiAl during composite consolidation, a reaction barrier coating of yttria was to be applied to the nickel-coated fiber using a solution coating process.

3.3 Nickel/Yttria Coatings

3.3.1 Experimental System. During the course of this project, an independent effort to develop a process for depositing nickel from nickel carbonyl was underway. The system used for that project was readily adapted to batch coating of the sapphire fibers. A schematic for the CVD system is shown in Figure 46. This reactor incorporates the required safety systems for working with $Ni(CO)_4$, such as special precursor containment and exhaust scrubbing systems. Transport of the $Ni(CO)_4$ was controlled using a peristaltic pump in conjunction with a digital scale. This configuration allowed a $Ni(CO)_4$ flow rate as low as 0.5 gram-per-minute (gpm). The $Ni(CO)_4$ was pumped into a vaporization chamber heated to 305K.

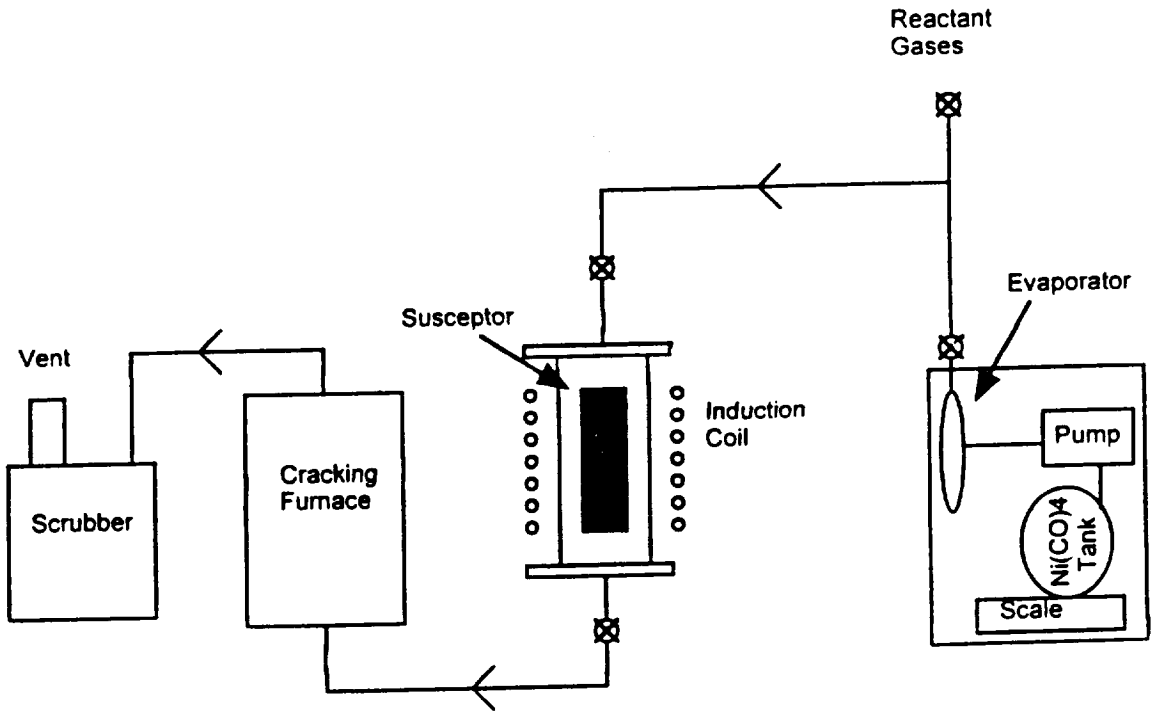

Figure 46. CVD Nickel System Schematic

The other process gases were mixed with the $Ni(CO)_4$ and distributed throughout the upper section of the reactor. The reactor consisted of a 30-centimeter long by 7.5-centimeter diameter quartz-vacuum chamber and a 5-centimeter diameter by 25-centimeter long stainless steel susceptor which was inductively heated. The fibers were drum-wound into tapes and suspended from the lid of the reactor. The substrate temperature was monitored using two type-K thermocouples placed inside the hot zone of the susceptor. The exhaust system consisted of a thermal cracking chamber and a scrubber, which had been specially modified to neutralize $Ni(CO)_4$. The entire processing system was contained in a walk-in hood which was maintained at a reduced pressure compared to the main laboratory. All of the process control systems were located outside of the walk-in hood to allow for remote operation.

The protective-Y_2O_3 coating was applied in a batch coating process using a yttrium nitrate hexahydrate ($Y(NO_3)_3 \cdot 6H_2O$ or YNH)/methanol solution which contained approximately 25 weight-percent YNH. The fibers were dipped into a beaker of the solution, allowed to air dry at ambient temperature for approximately one minute, and dried at 373K in air for one minute. The dried coatings were calcined in air for approximately two minutes at 1273K. This process was

repeated to produce a Y_2O_3 coating approximately 0.5 μm thick on top of the CVD nickel coating.

3.3.2 Yttria/Nickel Coating Development

The coating morphologies in the initial experiments were unacceptable. Generally the coatings had very large growth cones and a non-uniform distribution along the fiber length. The initial experiments were conducted between 423K and 473K at approximately 27.5 KPa (200 torr). Micrographs of the structure revealed that the growth cones were separated by voids, approximately 0.5 μm to 3 μm wide, at their base before the cones grew together. This morphology is typical of a high-substrate temperature that produces a limited number of nucleation sites which grow rapidly as cones until they eventually touch. During a series of development runs the $Ni(CO)_4$ flow, substrate temperature, and system pressure were systematically varied. These experiments showed that decreasing the substrate temperature, while increasing the system pressure, produced a more uniform coating.

Fully dense coatings were produced by lowering the substrate temperature to 403K flowing all process gases, except $Ni(CO)_4$, over the fibers, adjusting the substrate temperature to the selected value, and then introducing the reactant. Using this modified procedure, the substrate temperature only changed from 1K - 2K when the $Ni(CO)_4$ was introduced. The results of a 40-minute CVD run using this revised process is shown in Figure 47. The Ni coating is approximately 40-μm to 45-μm thick with a slightly faceted surface. This morephology indicates a slightly high deposition temperature. Lowering the deposition temperature to approximately 393K produced a much smoother coating (Figure 48). This coating is approximately 12-μm thick, not columnar, and moderately smooth. These final parameters were used to produce 30 meters of 3-μm, 5-μm, and 10-μm thick nickel coatings on sapphire fiber. A typical nickel-coated fiber, with the yttria solution coating, is shown in Figure 49. The solution coating process formed a rough yttria layer approximately 0.5 μm thick. The duplex-coated fibers were delivered to NASA-LeRC for testing and evaluation.

Figure 47. CVD Nickel Coating Produced in 40 Minutes

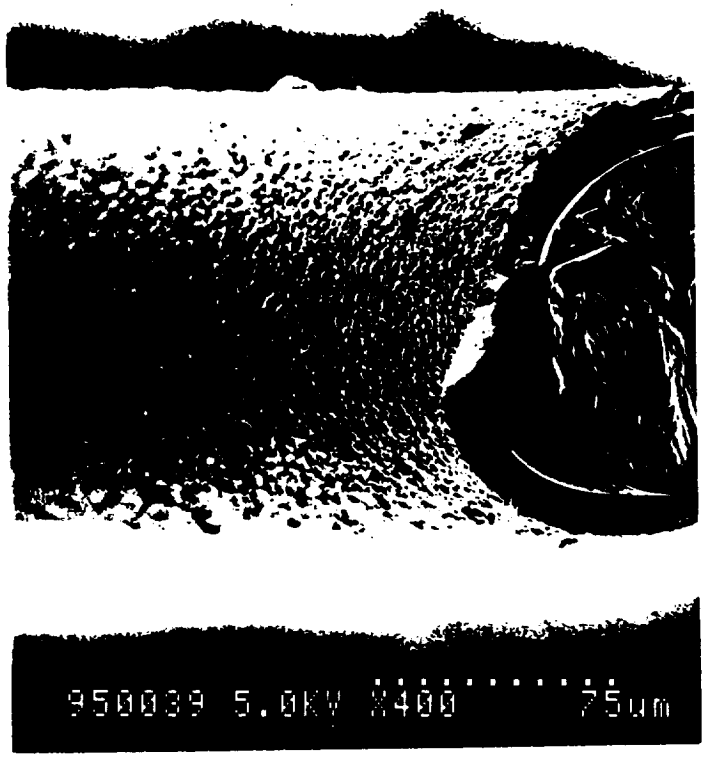

Figure 48. Nickel Coating Produced at 393K

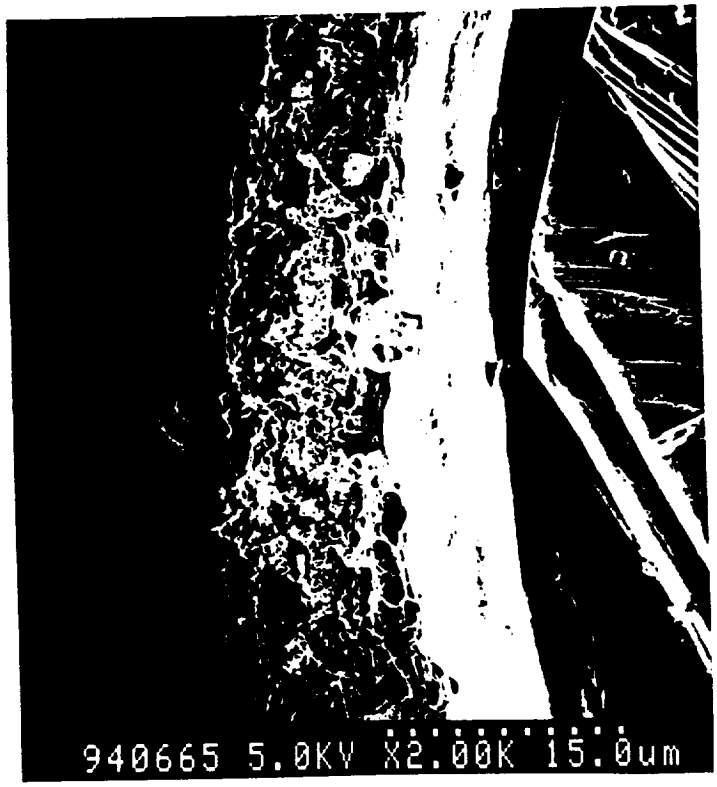

Figure 49. Nickel/Y_2O_3 Coating

4.0 CONCLUSIONS AND RECOMMENDATIONS

4.1 Conclusions

From the results of this program, the following conclusions can be drawn:

- Ni-Al compounds can be formed directly by MOCVD at temperatures as low as 523K.

- Mo deposition is practical for the production of thick (5 μm to 10 μm) coatings on fibers using molybdenum hexacarbonyl precursor and the two step process developed by Kmetz.

- An FGM reaction for the the NiAl-alumina system was difficult to develop because of the potential interaction of the precursors but may be possible with alternate nickel precursors.

- Nickel coatings can be deposited at high rate and may provide benefit for this or other MMC systems but the safety requirements of working with nickel carbonyl present significant capital expenses for a production system.

- Alumina coatings can be deposited at low temperatures using aluminum isopropoxide, and they do not degrade fiber strength in the as-deposited condition.

4.2 Recommendations

- Additional work is needed to characterize the effects of fiber coatings on the residual stress distribution in Al_2O_3/NiAl composites, and metal-matrix composites in general, and compare the results to the theoretical predictions. Understanding the effects

of fiber coatings is fundamental to applying IMC and MMC to aerospace components.

- The ability to form Ni-Al coatings by MOCVD at lower temperatures may allow the use of these materials as protective coatings for non-superalloy materials, including aluminum, copper, polymers, and their composites. This potential should be examined in future efforts.

- Future efforts on Ni-Al coatings should focus on the use of nickel carbonyl. Although its use presents serious safety requirements, nickel carbonyl offers the advantaages of simple transport and low deposition temperature.

5.0 FUTURE WORK

The Mo- and Ni-coated fiber produced in this project have been processed into NiAl composites by NASA- LeRC. The effect of the different coating materials and coating thicknesses on the residual stress in the composites will be investigated as part of a Doctoral research effort, which includes comparison of the residual stress distribution predictions of an existing concentric cylinder model to experimental measurements. The concentric cylinder model for residual stress modeling has been provided by Dr. Steven Arnold of NASA-LeRC. The residual stresses in the composites will be measured by neutron diffraction and nanohardness measurements. The neutron diffraction will be performed at Argonne National Laboratory (Dr. James Richardson) on the composites, as well as NiAl matrix powder, sapphire fibers, and Al_2O_3/NiAl baseline composites. Nanohardness measurements will be performed at BIRL.

******

This report is based upon data contained in BIRL Laboratory Record Books 195 and 257.

6.0 REFERENCES

1. J. W. Pickens, R.D. Noebe, G.K. Watson, P. K. Brindley, and S. L. Draper, "Fabrication of Intermetallic Matrix Composites by the Powder Cloth Process", NASA TM 102060, 1989.

2. R. R. Bowman, "Influence of Interfacial bond Strength on the Mechanical Properties of Continuous Fiber Reinforced NiAl Composites", in 5th Annual HiTEMP Review - 1992 NASA CP 10104 38-1 to 38-15.

3. A. K. Misra, K. S. Crandall, and R. R.Bowman, "Modification of Interface in Al_2O_3/NiAl Composite", in 5th Annual HiTEMP Review - 1992 NASA CP 10104 39-1 to 39-15.

4. C. A. Moose, D. A. Koss, and J. R. Hellman, "Interfacial Shear Behavior of Sapphire-Reinforced NiAl", *Mater. Res. Soc. Symp. Proc.* **194** 293-300 (1990)

5. R. D. Noebe, R. R. Bowman, and J. I. Eldridge, "Initial Evaluation of Continuous Fiber Reinforced NiAl", *Mater. Res. Soc. Symp. Proc.* **194** 323-332 (1990).

6. R.R. Bowman, and R. D. Noebe, "Processing and Mechanical Evaluation of Continuous Fiber Reinforced NiAl Composites", HiTEMP Review - 1990, NASA CP 10051, 40.1-40.14, (1991).

7. R. R. Bowman, R. D. Noebe, J. Doychak, K.S. Crandall, and I. E.Locci, "Effect of Interfacial Properties on the Mechanical Behavior of NiAl Based Composites", HiTEMP Review - 1991 , NASA CP 10082, 43.1-43.14 (1991).

8. P. K. Wright, M. D. Sensmeier, D. Kupperman, and H. Wadley, "Thermal Stress Effects in Intermetallic Matrix Composites", HiTEMP Review - 1991, NASA CP 10082, 45.1-45.14 (1991).

9. S. Majumdar, J. P. Singh, D. Kupperman, and A. D. Krawitz, "Application of Neutron Diffraction to Measure Residual Stains in Various Engineering Composite Materials", J.Eng. Mater. *Technol.*, **113** 51-9 (1991).

10. A. Saigal, and D. S. Kupperman, "Thermal Strains in Titanium Aluminide and Nickel Aluminide Composites", presented at Seventh World Conference on Titanium, San Diego, CA. June 28-July 2, 1992.

11. A. Saigal and D. S. Kupperman, "Residual Thermal Strains and Stresses in Nickel Aluminide Matrix Composites", *Scripta Metall. Mater.*, **25** 2547-2552 (1991).

12. R. D. Noebe, R. R. Bowman, and M. V. Nathal, "Review of the Physical and Mechanical Properties and Potential Applications of the B2 Compound NiAl", NASA Technical Memorandum 105598 April 1992.

13. S. M. Arnold, V. K. Arya, and M. E. Melis, "Reduction of Thermal Residual Stresses in Advanced Metallic Composites Based Upon a Compensating/Compliant Layer Concept", *J. Comp. Mat.*, **26** [9] 1287-1309 (1992).

14. S. Jansson and F.A. Leckie, "Reduction of Thermal Stresses in Continuous Fiber Reinforced Metal Matrix Composites with Interface Layers", *J. Comp. Mat.*, **26** [10] 1474-1486 (1992).

15. S. M. Arnold and T. E. Wilt, "Influence of Engineered Interfaces on Residual Stresses and Mechanical Response in Metal Matrix Composites", NASA Technical Memorandum 105438 1992.

16. M. Vedula, R. N. Pangborn, and R. A. Queeney, "Modification of Residual Thermal Stress in a Metal-Matrix Composite with the Use of a Tailored Interfacial Region", *Composites*, **19** [2] 133-137 (1988).

17. G. Z. Voyiadjis and C. S. Hartley, "Residual-Stress Determination of Concentric Layers of Cylindrically Orthotropic Materials", *Experimental Mechanics*, 290-7 September 1987.

18. S. Jansson and F. A. Leckie,"Reduction of Thermal Stresses in Continuous Fiber Reinforced Metal-Matrix Composites with Interface Layers",NASA Contractor Report 185302 October 1990.

19. B. N. Cox, M. R. James, D. B. Marshall, and R. C. Addison, Jr., "Determination of Residual Stresses in Thin Sheet Titanium Aluminide Composites", *Met. Trans. A* **21A** 2701-7 (1990).

20. A. J. Wilkinson, "Deformation Studies of Metal Matrix Composites using Electron Backscatter Patterns", *Mater. Sci. Eng.*, **A135** 189- 193 (1991).

21. A. K. Misra, "Thermodynamic Analysis of Compatibility of Several Reinforcement Materials with Beta Phase NiAl Alloys", NASA Contractor Report 4171 (1988).

22. H. F. Merrick and M. L. Labib, "Advanced Reinforcement Systems for Intermetallic Applications", Final Report under NASA Contract NAS 3-25970 March 1992.

23. I. F. Ferguson, J. B. Aincough, D. Morse, and A. W. Miller, "Decomposition of Molybdenum Hexacarbonyl", *Nature*, **202**, 1327-8 (1964).

24. M. Miyake, Y. Hirooka, T. Imoto, and T. Sano, "Chemical Vapour Deposition of Molybdenum on Graphite", *Thin Solid Films*, **79**, 75-81 (1981).

25. Y. Isobe, H. Shirakawa, P. Son, and M. Miyake, "Thermal Shock Resistance of Chemically Vapour-Deposited Molybdenum Coatings on Graphite", *J. Less Com. Metals*, **152**, 251-260 (1989).

26. Y. Isobe, S.Yamanaka, P. Son, and M. Miyake, "Structure and Thermal Resistance of Chemically Vapor Deposited Molybdenum on Graphite", *J. Vac. Sci. Technol. A*, **4** [6] 3046-9 (1986).

27. K. A. Gesheva, V. Abrosimova, and G. D. Beshkov, "CVD Carbonyl Thin Films of Tungsten and Molybdenum and Their Silicides - A Good Alternative to CVD Fluoride Tungsten Technology", *J. Physique IV C2*, **1** C2-865-71 (1991).

28. S. R. Nutt and F. E. Wawner, "CVD Coatings from Metal Carbonyls on SiC Filaments", Proceeding of the 5th Annual Conference on Composites and Advanced Ceramic Materials, edited by J. W. McCauley, AMERICAN CERAMIC SOCIETY, INC, Columbus, OH 1981.

29. J. J. Lander and L. H. Germer, "Plating Molybdenum, Tungsten, and Chromium by Thermal Decomposition of Their Carbonyls", *Am. Inst. of Min. and Met. Eng.*, **175**, 648-692 (1948).

30. L. H. Kaplan and F. M. d'Heurle, " The Deposition of Molybdenum and Tungsten Films from Vapor Decomposition of Carbonyls", *J. Electrochem. Soc.*, **117** [5] 693-700 (1970).

31. M. Kmetz, B. J. Tan, W. Willis, S. Suib, and F. S. Galasso, "CVD Mo, W, and Cr Oxycarbide, Carbide, and Silicide Coatings on SiC Yarn", *J. Mater. Sci.*, **26** 2107-2110 (1991).

32. A. I. DeRosa, D. B. Dove, and R. E. Loehman, "Properties of Molybdenum Films Prepared by Decomposition of the Carbonyl", *J. Vac. Sci. Technol.*, **11** [1] 455-7 (1974).

33. A. P. Patokin and V. V. Sagalovich, "Mass-Spectrometric Study of the Thermal Decomposition of Molybdenum and Tungsten Hexacarbonyls", *Russian J. Phys. Chem.*, **50** [3] 370-2 (1976).

34. W. T. Thompson, C. W. Bale, and A. D. Pelton, "FACT in Chemical Engineering", Proc. of 33rd Canadian Chem. Eng. Conf., Toronto, Canada October 1983.

35. M. Nino, and S. Maeda, "Recent Development Status of Functionally Gradient Materials", *ISIJ Internat.*, **30** [9] 699-703 (1990).

36. H. Takahashi, and T. Hashida, "Development of an Evaluation Method of Functionally Gradient Materials", *JSME Internat.Journal*, **33** [3] 281-7 (1990).

37. T. Hirai, and M. Sasaki, "Vapor-Deposited Functionally Gradient Materials", *JSME Internat. Journal*, **34** [2] 123-9 (1991).

38. J. A. Aboaf, "Deposition and Properties of Aluminum Oxide Obtained by Pyrolytic Decomposition of an Aluminum Alkoxide", *J. Electrochem. Soc.*, **114** [9] 948-952 (1967).

39. D. C. Bradley, "Metal Alkoxides as Precursors for Electronic and Ceramic Materials", *Chem. Rev.*, **89** 1317-1322 (1989).

40. M. T. Duffy, and W. Kern, "Chemical Vapor Deposition of Aluminum Oxide Films from Organo-Aluminum Compounds", *RCA Review*, **31** 754-770 (1970).

41. H. Mutoh, Y. Mizokami, H. Matsui, S. Hagiwara, and M. Ino, "Multilayer Metallization with Planar Interconnect Structure Utilizing CVD Al_2O_3 Film", *J. Electrochem. Soc.*, **122** [7] 987-992 (1975).

42. R. W. J. Morssinkhof, T. Fransen, M. M. D. Heusinkveld, and P. J. Gellings, "The Protective Properties of Thin Alumina Films Deposited by Metal Organic Chemical Vapour Deposition against High-Temperature Corrosion of Stainless Steels", *Mater. Sci. Eng.*, **A121** 449-455 (1989).

43. C. Dhanavantri, R. N. Karekar, and V. J. Rao, "Study of Graded Aluminum Oxide Films Prepared by Metal-Organic Chemical Vapor Deposition", *Thin Solid Films*, **127** 85-91 (1985).

44. R. W. J. Morssinkhof, T. Fransen, M. M. D. Heusinkveld, and P. J. Gellings, "Mechanistic Aspects of the Deposition of Thin Alumina Films Deposited by MOCVD", *Mat. Res. Soc. Symp. Proc.* **168** 125-130 (1990).

45. W.-P. Sun, H. J. Lin, and M.-H. Hon, "Kinetics of the Formation of Nickel Aluminide Coatings on Pure Nickel by Chemical Vapour Deposition", *Thin Solid Films*, **146** 55-64 (1987).

46. H. J. Lin, W. P. Sun, and M. H. Hon, "Gas Phase Aluminide Coatings on Nickel-Base Superalloy IN713", *Thin Solid Films*, **156** 259-264 (1988).

47. G. T. Stauf, D. C. Driscoll, P. A. Dowben, S. Barfuss, and M. Grade, "Iron and Nickel Thin Film Deposition via Metallocene Decomposition", *Thin Solid Films* **153** 421-430 (1987).

48. L. M. Dyagileva, O. N. Druzhkov, and Yu. A. Andrianov, "Gas-Phase Pyrolysis of Nickelocene", *Zhurnal Obshchei Khimii*, **47** [1] 82-85 (1977).

49. H. D. Kaesz, R. S. Williams, R. F. Hicks, J. I. Zink, Y.-J. Chen, H. J. Muller, Z. Xue, D. Xu, D. K. Shuh, and Y. K. Kim, "Deposition of Transition Metal and Mixed Metal Thin Films from Organometallic Precursors", *New J. Chem.*, **14** 527-534 (1990).